Synthesis and Characterization of Ruthenium Complexes which utilize a New Family of Terdentate Ligands based upon 2,6-Bis(pyrazol-1-yl)pyridine†

Carol A. Bessel,[a] Ronald F. See,[a] Donald L. Jameson,*[,b] Melvyn Rowen Churchill*[,a] and Kenneth J. Takeuchi*[,a]

[a] *Department of Chemistry, State University of New York at Buffalo, Buffalo, NY 14214, USA*

[b] *Department of Chemistry, Gettysburg College, Gettysburg, PA 17325-1486, USA*

To demonstrate the synthetic utility of a new family of terdentate ligands based on 2,6-bis(pyrazol-1-yl)pyridine (bpp), reaction conditions were developed to generate a variety of $[RuL(NO_2)(PMe_3)_2]^+$ complexes [L = bpp, 2,6-bis(3,5-dimethylpyrazol-1-yl)pyridine(bdmpp), 2,6-bis(3-phenylpyrazol-1-yl)pyridine (bppp) or 2,6-bis(3-*p*-chlorophenylpyrazol-1-yl)pyridine (bcppp)]. These complexes were characterized by elemental analysis, ^1H and ^{13}C NMR, infrared and UV/VIS spectroscopies, cyclic voltammetry, and single-crystal X-ray diffraction studies. The substituents of the terdentate bpp ligands sterically affected the Ru–N(pyrazole) bond lengths, the displacement of the nitrogen atoms of the nitro ligands from the RuL plane, and the twisting of the N–O vectors of the nitro ligand from that plane. Also the substituents affected the potentials and peak-current ratios of the Ru^{III}–Ru^{II} couples. The log (i_{pc}/i_{pa}) values (i_{pc} = cathodic peak current, i_{pa} = anodic peak current) are linearly correlated with the steric size of the substituents as estimated by Tolman's cone angles and with the distance of the nitro ligand out of the RuL plane. A linear correlation was also found between the differences in infrared absorbances due to the N–O symmetric and asymmetric stretches and the ratio of the N–O bond distances observed from the four crystal structures.

Polypyridyl ligands such as 2,2'-bipyridine (bipy) have been utilized with great frequency as ligands for transition-metal complexes.[1] In particular, bipy can stabilize a variety of oxidation states and co-ordination numbers with metal centres, and is often very stable towards redox reactions with high-oxidation-state metal centres. Also, due to the bidentate nature of bipy, this ligand is often resistant to dissociative ligand loss. Recently, there have been a number of studies involving complexes such as $[Ru(bipy)_3]^{2+}$, where the bipy ligand imparts useful photochemical and photophysical properties onto the ruthenium centre.[2] Again, the bidentate nature of bipy reduces the likelihood of photochemically induced ligand loss.

As a structural analogy to bipy, the terdentate ligand, 2,2':6',2''-terpyridine (terpy) has been the subject of a number of studies, involving a wide variety of metal centres.[3] Although terpy complexes often differ significantly from those of bipy, terpy is a very versatile ligand and a number of geometries and metal oxidation states have been observed.[4–12] In addition, due to the terdentate nature of terpy, it can occupy three meridional sites of a metal centre, and thus can be utilized to control and direct the reactivity of a transition-metal centre. In order to provide inorganic chemists with a new terdentate ligand which is structurally a terpy analogue, the family of ligands based on 2,6-bis(pyrazol-1-yl)pyridine (bpp) was developed. These new terdentate ligands are structurally similar to terpy, but are easier to modify synthetically.

With this paper we will establish that the family of bpp ligands [namely bpp, 2,6-bis(3,5-dimethylpyrazol-1-yl)pyridine (bdmpp), 2,6-bis(3-phenylpyrazol-1-yl)pyridine (bppp), and 2,6-bis(3-*p*-chlorophenylpyrazol-1-yl)pyridine (bcppp)] can be successfully incorporated within the co-ordination sphere of ruthenium. We will also examine the steric ligand effects of the bpp family of ligands through the potential values $E_{\frac{1}{2}}$ [$(E_{pc} + E_{pa})/2$] and the peak-current ratios, i_{pc}/i_{pa} (=cathodic peak current/anodic peak current[13]) of the Ru^{III}–Ru^{II} redox couples. Interestingly, the log (i_{pc}/i_{pa}) values correlate linearly with cone angle values[14] that are associated with the substituents of substituted bpp ligands (see below).

Since complete X-ray crystal structure determinations were conducted on four different ruthenium(II) complexes we also have a wealth of structural data concerning the structural effects of bpp ligands. In each complex a nitrite ligand is bonded in a monodentate fashion through the nitrogen atom (nitro co-ordination). These ruthenium(II) complexes maintain an octahedral ligand arrangement where two mutually *trans*-trimethylphosphine ligands exert a constant electronic influence and minimum steric influence on the nitro ligands, and only the substituents of the bpp ligand were changed. In addition to the above correlation between log (i_{pc}/i_{pa}) and cone angle, the former is also correlated linearly with the distance of the nitro ligand out of the plane of the terdentate ligand. There have been studies regarding the co-ordination of nitrite to transition metals, where a nitro–nitrito interconversion has been reported as the principal steric ligand effect on bound nitrite.[15] Notably, we do not observe such an interconversion with our complexes, but rather a novel nitro rotation in response to increased bpp steric size.

Experimental

Materials.—The ligands bpp, bdmpp, bppp and bcppp were prepared by literature methods or by slight modifications thereof.[16] The compound $RuCl_3 \cdot 3H_2O$ was obtained from Johnson Matthey Aesar/Alfa. Trimethylphosphine was purchased from Aldrich Chemical Co. as a 1.0 mol dm^{-3} solution in toluene or as a neat liquid. Ethylene glycol monoethyl ether was dried by distillation before use. All other solvents and materials were of reagent grade and were used without further purification. All reactions were conducted under N_2(g) unless otherwise noted.

† *Supplementary data available:* see Instructions for Authors, *J. Chem. Soc., Dalton Trans.*, 1993, Issue 1, pp. xxiii–xxviii.

Measurements.—Elemental analyses were performed by Atlantic Microlabs (Norcross, GA). Infrared spectra of Nujol mulls on NaCl plates were recorded with a Perkin Elmer 710B or a 1430 ratio recording spectrophotometer, electronic absorption spectra with a Milton Roy Spectronic 3000 diode-array spectrophotometer equipped with a Hewlett-Packard 7470A plotter or with a Bausch and Lomb Spectronic 2000 spectrophotometer equipped with a Houston Instruments model 200 recorder. Proton NMR spectra were recorded with a JEOL FX90Q Fourier-transform or a EM 390 spectrometer, ^{13}C NMR with either a JEOL FX90Q or a Varian Gemini 300 Fourier-transform spectrometer. Chemical shifts are reported in ppm relative to tetramethylsilane. Cyclic voltammetric experiments were carried out in a three-electrode, one-compartment cell equipped with a platinum working electrode (Bioanalytical Systems), a platinum auxiliary electrode and a saturated sodium chloride calomel reference electrode (SSCE). It was conducted with an IBM EC/225 polarographic analyser equipped with a Houston Instruments model 100 recorder. Methylene chloride or acetonitrile was utilized with 0.1 mol dm^{-3} tetrabutylammonium tetrafluoroborate as the supporting electrolyte (prepared by standard methods[17]).

X-Ray Data Collection.—Crystals were aligned on a Siemens-upgraded Syntex $P2_1/R3$ diffractometer equipped with a highly oriented graphite-crystal monochromator. The determination of the Laue symmetry, crystal class, unit-cell parameters and the crystal orientation matrix were carried out by previously described techniques.[18a] Room-temperature intensity data were collected with Mo-Kα radiation (λ = 0.710 73 Å), using the θ–2θ scan technique when possible, or the ω scan technique when peak overlap might otherwise be a problem. Details of data collection are in Table 3. All reflections in each data set were corrected for Lorentz and polarization effects and for absorption (semi empirical).

Solution and refinement of the structures. All crystallographic calculations were carried out on a VAX3100 workstation with the use of the Siemens SHELXTL PLUS[18b] program set. The analytical scattering factors for neutral atoms were corrected for both the $\Delta f'$ and the $i\Delta f''$ components of anomalous dispersion. The structures were solved by a combination of direct methods and Fourier-difference techniques. All non-hydrogen atoms were refined anisotropically, and hydrogen atoms were included in calculated positions with d(C–H) = 0.96 Å.[18c] Details of each structure solution and its refinement may be found in Table 3. Diagrams of the structures were generated using ORTEP II.[19]

Additional material available from the Cambridge Crystallographic Data Centre comprises H-atom coordinates, thermal parameters and remaining bond lengths and angles.

Preparations.—The complexes [Ru(bppp)Cl_3] **3**, *trans*-[Ru(bppp)Cl_2(PMe_3)] **7**, *cis*-[Ru(bppp)Cl_2(PMe_3)] **10** and *trans*-[Ru(bppp)Cl(PMe_3)$_2$] **13**, have been reported earlier.[20]

[RuLCl_3] (L = bpp **1**, bdmpp **2**, bppp **3** *or* bcppp **4**). A sample of $RuCl_3 \cdot 3H_2O$ (0.271 g, 1.0 × 10^{-3} mol) was combined with L (1.0–1.1 equivalents) in absolute EtOH (125 cm^3 for L = bpp) or in ethylene glycol monoethyl ether (125 cm^3 for L = bdmpp, bppp or bcppp). The solution was heated at reflux for 3 h. After cooling to room temperature, the precipitate was collected by vacuum filtration, washed thoroughly with absolute EtOH and Et_2O and air dried. These materials were used without purification in the following syntheses. Yields 85–90%.

trans-[RuLCl_2(PMe_3)] (L = bpp **5**, bdmpp **6**, bppp **7** *or* bcppp **8**). In a typical reaction, one of complexes **1**–**4** (0.120 g) was slurried in $CHCl_3$ or CH_2Cl_2 (15 cm^3), PMe_3 (1.5 equivalents) and triethylamine (2 cm^3) were added and the mixture was refluxed for 10–24 h. The resultant brown solid was collected by vacuum filtration, washed with the minimum volume of absolute EtOH and Et_2O and purified, if necessary, by passage through a short, deactivated (1 cm^3 distilled water, 10 cm^3 alumina) basic alumina column eluted with 2% (v/v) MeOH–CH_2Cl_2. The solvent of the red-brown product band was completely removed with a rotary evaporator. The residue was redissolved in CH_2Cl_2 and titurated into hexanes. A brown product was collected by vacuum filtration and used without further purification. Yields 55–90%.

cis-[RuLCl_2(PMe_3)] (L = bpp **9**, *or* bppp **10**). Complex **5** or **6** (0.1 g) was added to 1,2-dichloroethane (30–90 cm^3) and irradiated for 48–61 h with a 120 W tungsten light. The reactions were monitored by UV/VIS spectroscopy until no change occurred in the λ_{max} of the visible range. The reddish brown solution was filtered and the solvent of the filtrate was reduced to dryness by rotary evaporation. The solid was slurried in CH_2Cl_2 (4 cm^3) and titurated into hexanes or Et_2O (*ca.* 40 cm^3). The solid was collected by vacuum filtration and used without further purification. Yields 90–95%.

CAUTION: While the authors have used perchlorate as a counter ion with a number of ruthenium complexes without incident, perchlorate salts of metal complexes with organic ligands are potentially explosive. Care should be exercised in using a spatula or stirring rod mechanically to agitate any solid perchlorate. These complexes, as well as any other pechlorate salt, should be handled only in small quantities, using the appropriate safety procedures.[21]

trans-[RuL(Cl)(PMe_3)$_2$]ClO_4 (L = bpp **11**, bdmpp **12**, bppp **13** *or* bcppp **14**). *One-pot synthesis.* In a typical reaction, one of complexes **1**–**4** (1.0 g) was slurried in CH_2Cl_2 (300 cm^3), PMe_3 (4.5–7 equivalents) was added to the ruthenium suspension followed by Zn/Hg amalgam (12 g), and the mixture refluxed for 24 h before the heating mantle was removed. The mixture was then irradiated under a 120 W spot light for several days. The reactions were monitored for completion by UV/VIS spectroscopy. After filtering off the Zn/Hg amalgam and some insoluble green solids, the filtrate was reduced to dryness with a rotary evaporator. The orange residue was redissolved in the minimum volume of ethanol–water (40:60, v/v), solid $NaClO_4$ (2 g) added and the volume slowly reduced on a rotary evaporator. The yellow-orange solid was vacuum filtered and washed with the minimum volume of water. The product was purified by passing down a deactivated (1 cm^3 water, 10 cm^3 alumina) alumina column using acetone as the eluent. The initial orange band was collected and reduced to dryness on a rotary evaporator. The residue was redissolved in the minimum volume of acetone and titurated into Et_2O. The orange powder was washed with Et_2O and air dried. Yield 40–60% from **1**–**4**.

Alternative procedure for complex **11** *or* **13**. Complex **9** or **10** (0.020 g) was combined with 2 drops pure PMe_3 in acetone–EtOH (2:1, 15 cm^3), in an inert-atmosphere glove-box. The mixture was brought out of the glove-box and stirred in darkness, at room temperature, overnight. The solvent of the orange solution was completely removed using a rotary evaporator. The PF_6^- salt was isolated and purified as above. Yields 85–90% from **9** or **10**. ^1H NMR: **11** (300 MHz, $CDCl_3$), δ 0.7 (18 H, t, J = 3, PMe_3), 6.8 (2 H, s, pyrazolyl H), 7.8 (3 H, s, NC_5H_3), 8.1 (2 H, m, pyrazolyl H), 8.8 (2 H, s, pyrazolyl H) (t = second-order virtually coupled, 1:2:1 triplet); **12** (90 MHz, $CDCl_3$), δ 0.8 (18 H, t, J = 3, PMe_3), 2.6 (6 H, s, pyrazolyl Me), 2.9 (6 H, s, pyrazolyl Me), 6.3 (2 H, s, pyrazolyl H), 8.0 (3 H, m, NC_5H_3); **13** (90 MHz, $CDCl_3$), 0.8 (18 H, t, J = 3, PMe_3), 6.8 (2 H, d, J = 3, pyrazolyl H), 7.3 (6 H, m, *m*- and *p*-H of C_6H_5), 7.6 (4 H, m, *o*-H of C_6H_5), 8.1 (3 H, s, NC_5H_3), 8.8 (2 H, d, J = 3 Hz, pyrazolyl H); **14** (90 MHz, CD_3COCD_3), 0.9 (18 H, t, J = 4, PMe_3), 7.1 (2 H, d, J = 4, pyrazolyl H), 7.7 (8 H, dd, J = 16, 8, *o*- and *m*-H of C_6H_5), 8.3 (3 H, s, NC_5H_3) and 9.3 (2 H, d, J = 4 Hz, pyrazolyl H) (Found: C, 31.9; H, 4.2. $C_{17}H_{27}ClF_6N_5P_3Ru$ **11** requires C, 31.7; H, 4.2. Found: C, 40.5; H, 6.35. $C_{21}H_{35}Cl_2N_5O_4P_2Ru \cdot 0.75C_6H_{14}$ requires C, 40.8; H, 6.0. Found: C, 46.3; H, 4.7. $C_{29}H_{35}Cl_2N_5O_4P_2Ru$ **13** requires C, 46.4; H, 4.7. Found: C, 42.5; H, 4.0. $C_{29}H_{33}Cl_4N_5O_4P_2Ru$ requires C, 42.5; H, 4.05%).

trans-[RuL(NO_2)(PMe_3)$_2$]ClO_4 (L = bpp **15**, bdmpp **16**, bppp **17** *or* bcppp **18**). In a typical preparation, one of complexes

11–14 (0.10 g) was dissolved in 95% EtOH–water (50 : 50, v/v; 30 cm^3). Solid $NaNO_2$ (20 equivalents) was added to the orange solution and the mixture refluxed for 1–3 h. The yellow solution was reduced to 10 cm^3 on a rotary evaporator and solid $NaClO_4$ (1 g) was added. The resulting yellow solid was filtered off, washed with diethyl ether and air dried. The complexes were purified by elution through a deactivated (1 cm^3 water, 10 cm^3 alumina) alumina column using acetone as the eluent. The initial yellow band was reduced in volume and titurated into toluene. Yield 70–90%. The crystals for X-ray diffraction studies were prepared by slow evaporation over a period of days to weeks by the 'vial-within-a-vial' technique. For **15** and **16** a solution of acetone–cyclohexane was used while for **17** and **18** an EtOH–water mixture was used. NMR: ^1H, **15** (90 MHz, $CDCl_3$), δ 0.8 (18 H, t, J = 3, PMe_3), 6.9 (2 H, t, J = 3, pyrazolyl H), 8.3 (3 H, s, NC_5H_3), 8.4 (2 H, d, J = 3, pyrazolyl H), 8.9 (2 H, d, J = 3, pyrazolyl H); **16** (90 MHz, $CDCl_3$), δ 0.9 (18 H, t, J = 3, PMe_3), 2.4 (6 H, s, pyrazolyl Me), 3.0 (6 H, s, pyrazolyl Me), 6.4 (2 H, s, pyrazolyl H), 8.2 (3 H, m, NC_5H_3); **17** (90 MHz, $CDCl_3$), 0.7 (18 H, t, J = 3, PMe_3), 6.9 (2 H, d, J = 3, pyrazolyl H), 7.3 (6 H, m, *m*- and *p*-H of C_6H_5), 7.5 (4 H, m, *o*-H of C_6H_5), 8.2 (3 H, s, NC_5H_3), 9.0 (2 H, d, J = 3, pyrazolyl H); **18** (90 MHz, CD_3COCD_3), 0.8 (18 H, t, J = 4, PMe_3), 7.2 (2 H, d, J = 4, pyrazolyl H), 7.6 (8 H, dd, J = 35, 12, *m*- and *p*-H of C_6H_5), 8.4 (3 H, s, NC_5H_3), 9.4 (2 H, d, J = 4, pyrazolyl H); ^{13}C(300 MHz), **15** (CD_3COCD_3), δ 10.8 (t, J = 14), 109.0, 112.1, 133.4, 140.9, 146.8, 150.4; **16** ($CDCl_3$), 12.1 (t, J = 13), 13.6, 14.9, 108.1, 113.1, 140.8, 145.6, 149.2, 157.1; **17** ($CDCl_3$), 12.9 (t, J = 14), 107.9, 112.8, 115.3, 128.6, 128.7, 128.9, 130.6, 133.8, 148.1, 162.5; **18** (CD_3COCD_3), 12.9 (t, J = 14 Hz), 108.2, 112.9, 127.3, 129.2, 129.9, 134.0, 148.0, 161.5. IR(ν_{sym},ν_{asym}): **15**, 1300, 1320; **16**, 1270, 1290; **17**, 1300, 1330; **18**, 1290, 1330 cm^{-1} (Found: C, 33.6; H, 4.4. $C_{17}H_{27}ClN_6O_6P_2Ru$ **15** requires C, 33.5; H, 4.5. Found: C, 36.9; H, 5.4. $C_{21}H_{35}ClN_6O_6P_2Ru$ **16** requires C, 36.9; H, 5.5. Found: C, 45.4; H, 4.6. $C_{29}H_{35}ClN_6O_6P_2Ru$ **17** requires C, 45.7; H, 4.6. Found: C, 41.75; H, 4.0. $C_{29}H_{33}Cl_3N_6O_6P_2Ru$ **18** requires C, 41.9; H, 4.0%).

trans-$[RuL(NO)(PMe_3)_2][ClO_4]_3$ (L = bpp **19**, bdmpp **20**, bppp **21** *or* bcppp **22**). These reactions were not conducted under N_2(g). In a typical preparation, one of complexes **15–18** (0.025 g) was dissolved in acetone (2–5 cm^3). Three drops of 70% perchloric acid were added to the stirring solution causing an immediate colour change to light orange. After 2–3 min of stirring, diethyl ether (20 cm^3) was added to precipitate the yellow-orange complex. The product was filtered off, washed with diethyl ether and air dried. Yields 85–95%. IR(ν_{NO}): **19**, 1920; **20**, 1910; **21**, 1920; **22**, 1930 cm^{-1} (Found: C, 25.8; H, 3.4. $C_{17}H_{27}Cl_3N_6O_{13}P_2Ru$ **19** requires C, 25.8; H, 3.4. Found: C, 29.4; H, 4.2. $C_{21}H_{35}Cl_3N_6O_{13}P_2Ru$ **20** requires C, 29.7; H, 4.2. Found: C, 36.8; H, 3.8. $C_{29}H_{35}Cl_3N_6O_{13}P_2Ru$ **21** requires C, 36.9; H, 3.7. Found: C, 34.2; H, 3.3. $C_{29}H_{33}Cl_5N_6O_{13}P_2Ru$ **22** requires C, 34.35; H, 3.3%.

trans-$[Ru(bpp)(NO_2)(PMe_3)_2][AsF_6]_2$ **23**. This reaction was not conducted in N_2(g) and all reagents were first chilled in an ice-bath. Complex **15** (0.020 g, 3.35 × 10^{-5} mol) was dissolved in distilled water (4.5 cm^3). The oxidant, $[NH_4]_2[Ce(NO_3)_6]$ (0.367 g, 20 equivalents), was dissolved in the minimum of distilled water and added to the ruthenium solution. After 1 min, a solution of $LiAsF_6$ (1 g) dissolved in distilled water (1 cm^3) was added to precipitate the purple solid which was filtered immediately through a cold glass frit. The solid was washed with the minimum volume of cold water and allowed to air dry. Yields averaged 50%. The solid was stored in solid CO_2, and no elemental analysis was obtained.

Results and Discussion

This paper describes the preparation and characterization of a new series of *trans*-bis(phosphine)nitroruthenium complexes containing parent and substituted bpp ligands. The syntheses of these new complexes followed the general methods reported recently for Ru(bppp)Cl[20] and Ru(terpy)(NO_2) complexes,[22–24] with some important modifications. Longer reaction times and higher reaction temperatures were required to synthesise the Ru(bpp) complexes relative to the analogous (terpy) complex. However, we observed that even the sterically hindered bpp ligands such as bppp could be combined with ruthenium. This observation was unexpected and is particularly useful, because it is our experience that a sterically hindered terpy ligand, such as the 6,6″-diphenyl derivative cannot be utilized to form the $RuCl_3$ complex.[20]

NMR Spectroscopy.—Proton NMR spectroscopy of the *trans*-$[RuL(Cl)(PMe_3)_2]^+$ **11–14** and *trans*-$[RuL(NO_2)(PMe_3)_2]^+$ **15–18** complexes was utilized to determine the ligand arrangement about the ruthenium centre. The spectral data are consistent with terdentate bpp ligand co-ordination. A *trans*-phosphine arrangement, with overall C_{2v} symmetry of the cation, was suggested for all of the *trans*-$[RuL(Cl)(PMe_3)_2]ClO_4$ and *trans*-$[RuL(NO_2)(PMe_3)_2]ClO_4$ complexes.

The resonances for the methyl protons of the *trans*-PMe_3 ligands in both the *trans*-$[RuL(Cl)(PMe_3)_2]^+$ and *trans*-$[RuL(NO_2)(PMe_3)_2]^+$ complexes occurred between δ 0.7 and 0.9 in the ^1H NMR spectra. The complexes exhibited a 1 : 2 : 1 triplet due to virtual coupling of the phosphorus atoms where the coupling constant was 3–4 Hz. This strongly suggested the *trans* arrangement of the phosphine ligand.[25–28] The *trans*-phosphine arrangement, along with the C_{2v} symmetry of the cations, was corroborated by the crystal structures of the nitroruthenium(II) complexes.

The completely proton-decoupled ^{13}C NMR spectra of the *trans*-$[RuL(NO_2)(PMe_3)_2]^+$ cations also suggested an overall C_{2v} symmetry, consistent with an octahedral, *trans*-phosphine configuration. The spectra for these complexes displayed the appropriate number of resonances due to the unique carbon atoms of the bpp ligands. The resonances at δ 10.8–12.9 were assigned to the six chemically equivalent carbon atoms from the two phosphine ligands. These resonances were also split into a virtual triplet due to coupling with both phosphorus nuclei, with J = 3–4 Hz.

Infrared Spectroscopy.—The infrared spectra of the complexes **15–18** were used to investigate the bonding of the nitrite ligand. For all four complexes the nitrite ligand is in the *N*-bonded (nitro) configuration and assignments of ν_{asym}(asymmetric N–O stretch) and ν_{sym}(symmetric N–O stretch) were made by peak-by-peak inspection of the IR spectra of the *trans*-$[RuL(NO_2)(PMe_3)_2]ClO_4$ complexes in comparison to those of the *trans*-$[RuL(Cl)(PMe_3)_2]ClO_4$ precursors. Absorbances for the bpp family of complexes occurred between 1270 and 1300 cm^{-1} for the ν_{sym} and 1290 and 1330 cm^{-1} for the ν_{asym} N–O stretches. Interestingly, typical nitro complexes have $\nu_{sym}(NO_2)$ and $\nu_{asym}(NO_2)$ absorbances in the 1340–1320 and 1470–1370 cm^{-1} regions respectively, while nitrito complexes have two characteristic absorbances, ν(N=O) at 1485–1400 and ν(NO) at 1110–1050 cm^{-1}.[29–33] Although the IR absorbances observed for the bpp complexes have lower wavenumbers than those of most transition-metal nitro complexes,[33] these absorbances were consistent with *N*-bonding of the nitro ligand in *trans*-$[Ru(terpy)(NO_2)(PMe_3)_2]ClO_4$ (ν_{asym} 1324 and ν_{sym} 1297 cm^{-1}) for which an isotopic ($^{15}NO_2$) labelling study was reported.[23] For comparison, the free NO_2^- anion exhibits absorbances at 1250 and 1335 cm^{-1} (ν_{asym},ν_{sym} respectively).[15]

Notably, a linear correlation exists (slope = −0.046, R^2 = 0.99) between the ratio of the N–O bond distances and the differences in absorbance due to the symmetric and asymmetric N–O stretches. The bond-distance ratio = shorter N–O bond distance/longer N–O bond distance; and thus a ratio of unity is expected for nitro complexes. This correlation shows that the N–O bond-distance ratios decrease (the bonds become more inequivalent in length) as the differences in the infrared

Table 1 The UV/VIS spectral data for $RuL(PMe_3)$ complexes

Complex	λ_{max}/nm (10^{-3} ε/dm^3 mol^{-1} cm^{-1})[a]
5 *trans*-[Ru(bpp)$Cl_2(PMe_3)$]	468(4.7), 343(2.6), 307(22.5), 291(sh), 275(17.0), 265(sh)
6 *trans*-[Ru(dmbpp)$Cl_2(PMe_3)$]	470 (5.2), 313 (25.9), 271 (29.9)
7 *trans*-[Ru(bppp)$Cl_2(PMe_3)$][b]	495 (3.4), 364 (2.9), 326 (14.7), 316 (sh), 292 (19.3)
8 *trans*-[Ru(bcppp)$Cl_2(PMe_3)$][b]	494 (4.3), 327 (23.7), 292 (49.6)
9 *cis*-[Ru(bpp)$Cl_2(PMe_3)$]	446 (3.7), 408 (sh), 300 (12.3), 272 (14.6), 267 (sh)
10 *cis*-[Ru(bppp)$Cl_2(PMe_3)$][b]	483 (5.2), 319 (19.2), 292 (25.8)
11 *trans*-[Ru(bpp)Cl$(PMe_3)_2$]ClO_4	426 (3.8), 386 (sh), 283 (23.7), 269 (27.6)
12 *trans*-[Ru(bdmpp)Cl$(PMe_3)_2$]ClO_4	427 (6.4), 315 (22.8), 390 (sh), 270 (38.6)
13 *trans*-[Ru(bppp)Cl$(PMe_3)_2$]ClO_4[b]	434 (6.2), 320 (24.1), 284 (37.7)
14 *trans*-[Ru(bcppp)Cl$(PMe_3)_2$]ClO_4	426 (6.4), 320 (22.9), 292 (49.7)
15 *trans*-[Ru(bpp)$(NO_2)(PMe_3)_2$]ClO_4[c]	368 (6.1), 303 (18.8), 292 (sh), 271 (27.3), 262 (sh)
16 *trans*-[Ru(bdmpp)$(NO_2)(PMe_3)_2$]ClO_4[c]	391 (4.3), 314 (23.8), 306 (sh), 272 (33.0), 264 (sh)
17 *trans*-[Ru(bppp)$(NO_2)(PMe_3)_2$]ClO_4[c]	397 (4.2), 324 (23.9), 283 (41.7)
18 *trans*-[Ru(bcppp)$(NO_2)(PMe_3)_2$]ClO_4[c]	408 (4.3), 329 (25.6), 290 (49.6)
19 *trans*-[Ru(bpp)$(NO)(PMe_3)_2$]$[ClO_4]_3$[c]	361 (2.9), 300 (sh), 250 (27.9)
20 *trans*-[Ru(bdmpp)$(NO)(PMe_3)_2$]$[ClO_4]_3$[c]	361 (2.9), 300 (sh), 250 (26.4)
21 *trans*-[Ru(bppp)$(NO)(PMe_3)_2$]$[ClO_4]_3$[c]	382 (3.0), 326 (sh), 277 (34.0)
22 *trans*-[Ru(bcppp)$(NO)(PMe_3)_2$]$[ClO_4]_3$[c]	390 (3.0), 328 (sh), 280 (34.0)
23 *trans*-[Ru(bpp)$(NO_2)(PMe_3)_2$]$[AsF_6]_2$[c]	363 (1.0), 321 (3.2), 300 (5.8), 262 (11.6), 216 (16.5)

[a] Spectra were taken in CH_2Cl_2; sh = shoulder. [b] Reported in ref. 20. [c] Spectrum taken in MeCN.

absorbances increase towards the N–O single- and double-bond frequencies observed for nitrito compounds such as MeONO. A linear correlation exists for complexes of Ni, Zn, Cu and Co containing chelated, asymmetrically chelated, monodentate nitrito and bridging nitrite groups[15] and our study now extends this phenomenon to nitro complexes of ruthenium. Also, the differences in the absorbances due to the N–O stretches and the inequality of the N–O bond lengths increase as the substituents on the bpp ligand increase in size. The bpp ligand provides the greatest equality in N–O bond distances and the smallest difference in symmetric and asymmetric N–O stretching modes followed by bdmpp, bppp and bcppp respectively. This ordering is also observed regarding the stability of the electrochemically generated nitroruthenium(III) complexes (see below).

The infrared spectra of the *trans*-$[RuL(NO)(PMe_3)_2][ClO_4]_3$ **19–22** complexes suggested linear NO^+ ligands with ν_{NO} in the region of 1910–1930 cm^{-1}. This was consistent with the linear NO range of Haymore and Ibers[34] (ν_{NO} above 1620–1610 cm^{-1} were assigned to linear M–N–O systems, while ν_{NO} below 1610 cm^{-1} were assigned to bent M–N–O systems).

Electronic Spectroscopy.—The ultraviolet–visible transitions of the $RuL(PMe_3)$ complexes are given in Table 1. For *trans*-$[RuLCl_2(PMe_3)]$ **5–8** the transitions in the range of 495–470 nm were assigned to $d_\pi(Ru) \longrightarrow \pi^*(L)$ metal-to-ligand charge-transfer (m.l.c.t.) bands as observed for other *trans*-phosphineruthenium(II) complexes.[35–39] The lower-wavelength transition (< 400 nm) were assigned as $\pi \longrightarrow \pi^*$ ligand-localized transitions, in analogy to those for other reported Ru(terpy) complexes.[36–40] The transitions with low absorption coefficients (ε < 3000 dm^3 mol^{-1} cm^{-1}) at 343 and 364 nm for complexes **5** and **7**, respectively, could also be assigned to d–d transitions in analogy to other ruthenium(II) complexes with strong-field ligands.

The addition of a second phosphine to form the *trans*-$[RuL(Cl)(PMe_3)_2]^+$ **11–14** complexes and the change from a neutral to a positively charged complex resulted in a shift of all of the m.l.c.t. transitions to shorter wavelengths. Complexes **11–14** demonstrated a shift of 80–100 nm to shorter wavelengths for the m.l.c.t. transitions on substitution of the chloride ligand for trimethylphosphine. This was less than the decrease of 142 nm observed for the change from *trans*-$[Ru(terpy)Cl_2(PMe_3)]$ to *trans*-$[Ru(terpy)Cl(PMe_3)_2]^+$.[23] Those transitions at wavelengths < 350 nm were again assigned to $\pi \longrightarrow \pi^*$ ligand-localized transitions by analogy to Ru(terpy) complexes.[36–40]

The UV/VIS spectra of *trans*-$[RuL(NO_2)(PMe_3)_2]^+$ **15–18** complexes contained three absorbances. The shift to shorter wavelengths upon substitution of the Cl^- ligand by the NO_2^- ligand was consistent with the observed increase in the potentials of the Ru^{III}–Ru^{II} couple of **15–18** relative to those of **11–14**. The visible wavelength transitions of the *trans*-$[RuL(NO_2)(PMe_3)_2]^+$ complexes were 42–82 nm lower than those of the analogous *trans*-$[Ru(terpy)(NO_2)(PMe_3)_2]^+$ complex.[23]

The electronic spectrum of *trans*-$[Ru(bpp)(NO_2)(PMe_3)_2][AsF_6]_2$ **23** showed a shift in the m.l.c.t. transitions to shorter wavelengths due to the increase in charge of the complex (over that of **15**). This shift resulted in no visible transitions. The ultraviolet spectrum was composed of complicated and unresolved overlapping absorbances.

Cyclic Voltammetry.—Table 2 lists the $E_{\frac{1}{2}}$ potentials, ΔE_p and i_{pc}/i_{pa} ratios for the newly synthesised phosphineruthenium-(II) and -(III) complexes. The *trans*-$[RuLCl_2(PMe_3)]$ **5–8**, *cis*-$[RuLCl_2(PMe_3)]$ **9**, **10** and *trans*-$[RuL(Cl)(PMe_3)_2]^+$ **11–14** complexes all displayed one reversible Ru^{III}–Ru^{II} couple. Fig. 1 demonstrates the cyclic voltammetry associated with *trans*-$[RuL(NO_2)(PMe_3)_2]^+$ complexes. Initiating each scan at 0.0 V *vs.* SSCE, an oxidative wave was present for all complexes at *ca.* +1.0–1.3 V *vs.* SSCE corresponding to the oxidation of the ruthenium centre to ruthenium(III). Notably, oxidation of the nitroruthenium(II) complexes occurred without substantial decomposition only in the case of **15** [Fig. 1(*a*)]. For cyclic voltammograms (*b*)–(*d*) of Fig. 1 the reductive peak current corresponding to the interconversion of nitroruthenium-(III) to -(II) was much smaller than the oxidative peak current. This decrease indicated decomposition of the nitroruthenium(III) complexes. Furthermore, a reversible couple at *ca.* +0.3–0.45 V was present once the nitroruthenium(II) complexes, **16–18**, were oxidized. By comparison with authentic samples, this reversible wave at +0.3–0.45 V was assigned to the formation of the *trans*-$[RuL(NO)(PMe_3)_2]^{3+}$ complex.[23,32,41] We believe that the decomposition of the $[RuL(NO_2)(PMe_3)_2]^{2+}$ complexes follows the pathways postulated by Meyer[41] based on cyclic voltammetry at much higher scan rates. A further investigation of the rates and mechanisms of decomposition of $[RuL(NO_2)(PR_3)_2]^{2+}$ complexes is currently underway.[42]

The stabilities of the nitroruthenium(III) complexes were quantified primarily through i_{pc}/i_{pa} ratios obtained through cyclic voltammetry experiments.[13] For example, the *trans*-$[Ru(terpy)(NO_2)(PMe_3)_2]^+$ and *trans*-$[Ru(bpp)(NO_2)(PMe_3)_2]^+$ complexes had i_{pc}/i_{pa} ratios of 0.90 and 0.86:1 respectively. These i_{pc}/i_{pa} ratios indicated the terpy complex was

Table 2 Potentials $E_{\frac{1}{2}}$, ΔE_p and i_{pc}/i_{pa} for $Ru^{II}L(PMe_3)$ complexes

Complex	$E_{\frac{1}{2}}$[a]/V *vs.* SSCE	ΔE_p/V	i_{pa}/i_{pc}[b]
5	+0.42	0.11	
6	+0.32	0.16	
7[c]	+0.41	0.08	
8	+0.46	0.08	
9	+0.65	0.08	
10[c]	+0.56	0.08	
11	+1.00	0.10	
12	+0.91	0.14	
13[c]	+0.94	0.14	
14	+1.02	0.15	
15[d]	+0.14	0.12	0.86
16[d]	+1.07	0.16	0.47
17[d]	+1.18[e]	—	0.20
18[d]	+1.22[e]	—	0.21
19[d]	+0.31	0.05	
	−0.40	0.05	
20[d]	+0.34	0.10	
	−0.56	0.10	
21[d]	+0.40	0.05	
	−0.30	0.05	
22[d]	+0.45	0.06	
	−0.25	0.11	
23[d,f]	+1.13	0.06	

[a] Conditions: 0.1 mol dm^{-3} NBu_4BF_4 in CH_2Cl_2; platinum working electrode; SSCE reference electrode; scan rate 100 mV s^{-1}. $E_{\frac{1}{2}} = (E_{p,anodic} + E_{p,cathodic})/2$; $\Delta E_p = (E_{p,anodic} - E_{p,cathodic})$. [b] The i_{pc}/i_{pa} (where i_{pc} = cathodic peak current and i_{pa} = anodic peak current) ratios were obtained through the steady-state method of cyclic voltammetry.[14] The estimated error associated with these measurements is less than 20%. [c] Reported in ref. 20. [d] 0.1 mol dm^{-3} NBu_4BF_4 in MeCN. [e] Cyclic voltammogram was irreversible; E_p is for the anodic wave. [f] Cyclic voltammogram was taken in solid CO_2–chlorobenzene bath; −39 °C.

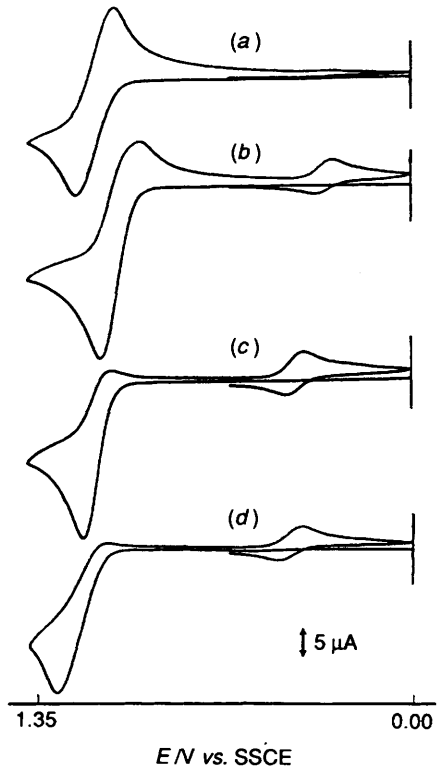

Fig. 1 Cyclic voltammograms in 0.1 mol dm^{-3} NBu_4BF_4 in acetonitrile at a platinum working electrode *versus* SSCE at a scan rate of 100 mV s^{-1}: (*a*) $[Ru(bpp)(NO_2)(PMe_3)_2]ClO_4$ **15**, (*b*) $[Ru(bdmpp)(NO_2)(PMe_3)_2]ClO_4$ **16**, (*c*) $[Ru(bppp)(NO_2)(PMe_3)_2]ClO_4$ **17** and (*d*) $[Ru(bcppp)(NO_2)(PMe_3)_2]ClO_4$ **18**

slightly more stable to oxidation than the corresponding bpp complex. When the two nitroruthenium(II) complexes were oxidized chemically and isolated that containing the terpy ligand was more thermally stable than the bpp complex, being easily handled at room temperature. Thus i_{pc}/i_{pa} ratios were a useful measure of the stability of the chemically generated oxidized species.

Steric effects were first recognized as important in reactivity and equilibrium studies of organic reactions.[43] For transition-metal complexes, the most frequently employed measure of the steric properties of phosphorus and related ligands has been the cone angle, θ, developed by Tolman. Tolman defined θ as the angle which defines a cone, 2.28 Å from the centre of the P atom, which touches the outermost van der Waals radii of the substituent atoms in a Corey–Pauling–Koltun (CPK)[44] molecular model.[14] Although cone angle parameters have been used extensively to correlate the steric size of phosphine ligands to the rate constants of ligand substitution, CO infrared stretching frequencies, and NMR chemical shifts, similar parameters are not available in terms of multidentate pyridine-based ligands. Thus, as a first approximation of the *relative* steric size of the substituted bpp ligands, we utilized Tolman's cone angle values directly. For bpp (where the substituent is H) we used the cone angle of the PH_3 ligand (87°), for bdmpp (Me substituted) we used the cone angle for trimethyl-substituted phosphine (PMe_3, 118°), for bppp (Ph substituted) and bcppp (*p*-ClC_6H_4 substituted) we used the cone angle value of triphenyl-substituted phosphine (PPh_3, 145°). Even though θ was originally established for phosphine ligands, the log (i_{pc}/i_{pa}) ratios for the terdentate bpp ligands were linearly correlated (slope = −0.011 deg^{-1}, R^2 = 0.99) with the *relative* increases in steric size observed with θ. This correlation led us to conclude that increasing the steric size of the substituents on the bpp ligands causes the instability of the electrochemically generated nitroruthenium(III) complexes.

The log (i_{pc}/i_{pa}) ratios also produced a linear correlation (slope = −5.6 $Å^{-1}$, R^2 = 0.93) with the distance of the nitro ligand out of the RuL plane. Movement of the co-ordinated nitrogen of the nitro ligand away from the meridional co-ordination plane (defined by the three co-ordinating nitrogens of the terdentate ligand) is another mechanism which might relieve steric crowding. In **15**, which has no substituents, the nitrogen atom of the nitro ligand is found precisely in the meridional co-ordination plane. In **16**, which has methyl substituents, the nitrogen atom of the nitrite ligand is displaced only 0.012 Å from the meridional plane. In **17** and **18**, with bulky groups (phenyl and *p*-chlorophenyl, respectively) as substituents, the nitrogen atoms of the nitrite groups are displaced by 0.100 and 0.091 Å, respectively. This correlation indicates that the stability of the nitroruthenium(III) complexes decreases as the distance of the nitro ligand out of the plane increases. While the decomposition of nitroruthenium(III) complexes has been studied extensively in terms of product distributions,[32,41] these two correlations [namely log (i_{pc}/i_{pa}) *vs.* θ and *vs.* distance of the nitro nitrogen from the meridional plane] allow us to offer new insight into the underlying cause of this decomposition. We postulate that, for these complexes, the cause of nitroruthenium(III) decomposition is primarily steric in nature.

Crystal Structure Analysis.—The crystal structures of complexes **15**, **16**·H_2O, **17**, and **18**·0.5H_2O consisted of ordered arrays of ruthenium cations and ClO_4^- anions in a 1:1 stoichiometry. Two of the crystal structures also revealed water of hydration. The experimental data for these X-ray diffraction studies are collected in Table 3. Atomic coordinates for all four structures are given in Tables 4–7. The perchlorate anions in the structures of **15** and **17** suffer from disorder.

trans-$[Ru(bpp)(NO_2)(PMe_3)_2]ClO_4$ **15**. Interatomic distances and angles and their estimated standard deviations

Table 3 Experimental data for the crystallographic studies*

Compound	**15**	**16**·H_2O	**17**	**18**·0.5H_2O
Empirical formula	$C_{17}H_{27}ClN_6O_6P_2Ru$	$C_{21}H_{35}ClN_6O_6P_2Ru\cdot H_2O$	$C_{29}H_{35}ClN_6O_6P_2Ru$	$C_{29}H_{33}Cl_3N_6O_6P_2Ru\cdot 0.5H_2O$
Formula weight	609.9	684.0	762.1	840.0
Colour, habit	Lemon-yellow crystal	Lemon-yellow crystal	Yellow crystal	Yellow-green crystal
Crystal size (mm)	0.35 × 0.3 × 0.3	0.3 × 0.3 × 0.25	0.4 × 0.4 × 0.5	0.4 × 0.35 × 0.3
Crystal system	Tetragonal	Orthorhombic	Monoclinic	Monoclinic
Space group	$P\bar{4}2_1m$	$P2_12_12_1$	$P2_1/n$	Pc
a/Å	9.5890(10)	9.370(2)	9.9420(10)	15.249(2)
b/Å		9.803(2)	24.073(4)	10.168(2)
c/Å	13.525(2)	32.860(11)	14.303(2)	23.360(3)
β/°			93.32(1)	93.49(1)
U/Å^3	1243.6(4)	3018.3(14)	3417.3(9)	3615.3(9)
Z	2	4	4	4
D_c/Mg m^{-3}	1.629	1.501	1.481	1.543
μ/mm^{-1}	0.895	0.748	0.667	0.784
F(000)	620	1404	1560	1708
2θ Range/°	5.0–50.0	5.0–45.0	8.0–50.0	5.0–50.0
Scan type	2θ–θ	ω	ω	2θ–θ
Scan speed/° min^{-1}	Constant, 1.75	2.00	2.76	3.00
Scan range (ω/°)	0.48° plus Kα separation	0.70	0.60	0.50
h,k,l	−11 to 0, −11 to 11, −16 to 16	0–10, 0–10, −35 to 35	−12 to 12, 0–29, −18 to 18	−18 to 18, 0–12, −27 to 27
Reflections collected	4714	4496	12 360	13 572
Independent reflections (R_{int} in %)	1212 (0.78)	3960 (0.85)	6026 (1.7)	12 780 (2.4)
Reflections > 6σ	1155	3138	4286	8716
Minimum, maximum transmission	0.5328, 0.5767	0.6758, 0.7222	0.6225, 0.6382	0.6555, 0.6914
Absolute structure, η	1.06(9)	1.04(8)	Not applicable	1.08(7)
Hydrogen atoms	Riding model, refined isotropic U	Fixed isotropic U	Fixed isotropic U	Fixed isotropic U
Extinction correction, χ	0.000 07(5)	0.000 48(11)	0.000 40(9)	0.000 08(4)
Weighting scheme, w^{-1}	$\sigma^2(F) + 0.0007F^2$	$\sigma^2(F) + 0.0016F^2$	$\sigma^2(F) + 0.0008F^2$	$\sigma^2(F) + 0.0027F^2$
Number of parameters refined	109	344	419	855
Final indices R,R' (all data)	0.0210, 0.0292	0.0471, 0.0523	0.0550, 0.0540	0.0677, 0.0683
(6σ data)	0.0196, 0.0282	0.0332, 0.0462	0.0352, 0.0474	0.0425, 0.0569
Goodness-of-fit	0.97	0.96	1.19	0.85
Largest and mean Δ/σ	0.011, 0.001	0.001, 0.000	0.009, 0.001	0.014, 0.000
Data-to-parameter ratio	11.1:1	11.5:1	14.4:1	14.9:1
Largest difference peak, hole/e Å^{-3}	0.47, −0.32	0.84, −0.80	0.55, −0.50	0.99, −0.87

* Details in common: background measurement, stationary crystal–stationary counter at beginning and end of scan, each for 25% of total scan time; three standard reflections every 97; full-matrix least-squares refinement; quantity minimized $\Sigma w(F_o - F_c)^2$; $F^* = F[1 + (0.002\chi F^2/\sin 2\theta)]^{-\frac{1}{4}}$.

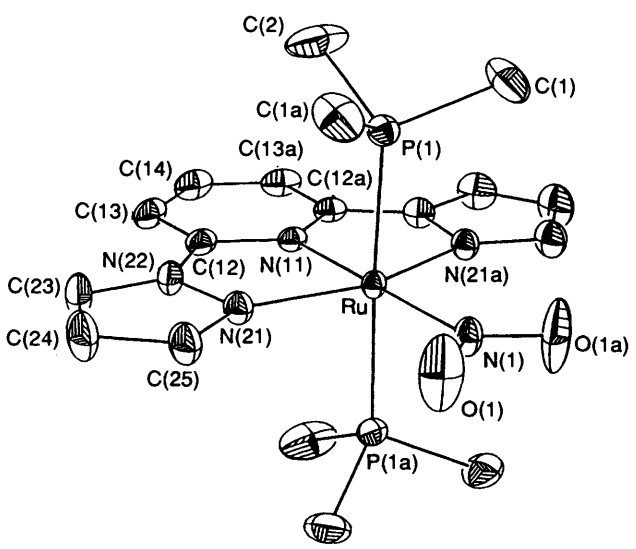

Fig. 2 An ORTEP II view of $[Ru(bpp)(NO_2)(PMe_3)_2]ClO_4$ **15**

(e.s.d.s) are listed in Table 8. A perspective view of the molecule, with the atomic numbering scheme, is shown in Fig. 2. The crystal structure confirmed the C_{2v} symmetry assigned to this complex. It is important to note that the ruthenium atom lies at the intersection of two mirror planes, one of which contains all atoms of the bpp ligand, while the other contains the phosphorus atoms of the PMe_3 ligands and the nitrogen atom of the nitro ligand [Ru–NO_2 2.058(4) Å]. The angles Ru(1)–N(1)–O(1) and Ru(1)–N(1)–O(1a) are each 122.9(2)°, and all atoms of the nitro ligand are contained in the plane of the ruthenium atom and all atoms of the bpp ligand. The angle O(1)–N(1)–O(1a) is 114.1(5)°. The O–N–O angles of all four nitro complexes reported here are in the middle of the range (113–127°) of those in nitro complexes of such transition metals as Co, Ni, Cu, Pd, Pt and Ru.[45,46]

The symmetry of this molecule requires that the two trimethylphosphine ligands be directly opposite each other, where the P(1)–Ru–P(1a) bond angle is 176.0(1)°. The observed Ru–P bond distances are 2.360(1) Å and are within the range of 2.26–2.41 Å reported for other Ru–P complexes.[23,45–51] The bpp ligand is bound to the three remaining co-ordination sites in a meridional fashion through three of the nitrogen atoms. The central pyridine fragment of the terdentate ligand is

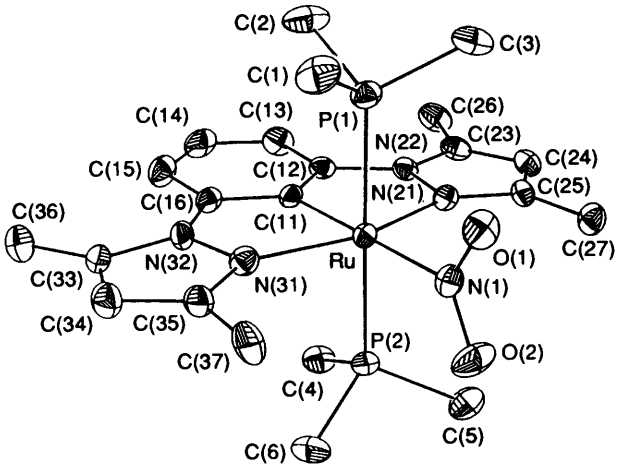

Fig. 3 An ORTEP II view of $[Ru(bdmpp)(NO_2)(PMe_3)_2]ClO_4$ **16**

bound *trans* to the nitro ligand, with Ru–N(11) 1.990(3) Å. The Ru–N(central pyridine) bond length in $[Ru(terpy)(NO_2)(PMe_3)_2]ClO_4$ and in all of the $[RuL(NO_2)(PMe_3)_2]ClO_4$ complexes are within 0.01 Å of 1.99 Å. These values can be compared to those of the $[Ru(bipy)_3]^{2+}$ complex where the average Ru–N(bipy) bond distance is 2.056 Å and of $[Ru(py)_6]^{2+}$ (py = pyridine) where the average Ru–N(pyridine) bond distance is 2.12 Å.[52] Finally, the constraints of the bpp ligand result in a significant deviation from a regular octahedral co-ordination geometry, as is shown by the Ru–N(21) and Ru–N(21a) bond lengths of 2.070(3) Å [some 0.080 Å longer than the Ru–N(11) distance of 1.990(3) Å] and the acute N(11)–Ru–N(21) and N(11)–Ru–N(21a) bond angles of 78.6(1)°.

trans-$[Ru(bdmpp)(NO_2)(PMe_3)_2]ClO_4 \cdot H_2O$ **16**·H_2O. Interatomic distances and angles are given in Table 9 and the molecule is illustrated in Fig. 3. This crystal consists of an array of ruthenium-containing cations and perchlorate anions with one H_2O solvent molecule for each cation–anion pair. The Ru–N(nitro) bond distance of 2.087(5) Å is similar to that [2.074(6) Å] reported for *trans*-$[Ru(terpy)(NO_2)(PMe_3)_2]ClO_4$.[23] The N–O bond distances are 1.247(7) and 1.243(8) Å, and the O(1)–N(1)–O(2) bond angle of 117.0(5)° is within the normal range for transition-metal nitro complexes.[45,46] These bond distances and angles can be compared to that of the free nitrite ion. In $NaNO_2$ the N–O bond distance was found to be 1.240(3) Å and the O–N–O angle 114.9(5)°.[53,54] Our crystal structure supports the conclusions of Hitchman and Rowbottom[15] on the *N*-bonding (nitro) of the nitrite ligand. They suggested that co-ordination of a nitro ligand has little effect on the N–O bond lengths (ours were the same within error). Further that the nitro bonding mode caused a significant opening of the O–N–O angle, by about 2°, on co-ordination to a divalent metal ion.[15] We have observed an opening of 2.1°.

The Ru–N(1)–O angles are 121.0(4)° for O(1) and 121.9(4)° for O(2). Notably, while the nitro ligand of **15** lies in the plane of the terdentate bpp ligand, the nitro group of **16** is oriented so that it lies almost perpendicular to the meridional co-ordination plane of the bdmpp ligand. The angle between the nitro ligand plane and the meridional co-ordination plane is 88.1°, with the nitrogen atom of the nitro ligand being displaced by 0.012 Å from the meridional co-ordination plane. The two trimethylphosphine ligands are almost directly *trans* to one another, the P(1)–Ru–P(2) angle being 178.4(1)°.

The N–Ru–N angles between the nitrogen of the pyridine fragment [N(11)] and the co-ordinating nitrogen atoms of the pyrazole fragments [N(21) and N(31)] show contractions from the regular octahedral value of 90° due to the geometric constraints of the terdentate ligand, with N(11)–Ru–N(21) 78.2(2) and N(11)–Ru–N(31) 78.9(2)°. Evidence of steric strain is also seen in the Ru–N bond lengths, where that to the central pyridine fragment [Ru–N(11)] is 1.992(4) Å and those to the pyrazole fragments are longer, 2.071(5) and 2.068(6) Å. The Ru(bdmpp) moiety is not quite planar, with the ruthenium(II) atom 0.022 Å out of the meridional co-ordination plane of the bdmpp ligand.

Table 4 Atomic coordinates ($\times 10^4$) for *trans*-$[Ru(bpp)(NO_2)(PMe_3)_2]ClO_4$ **15**

Atom	*x*	*y*	*z*
Ru	10 000	5 000	8 180(1)
P(1)	8 261(1)	6 739(1)	8 240(1)
C(1)	8 793(5)	8 313(4)	8 879(4)
C(2)	7 620(5)	7 380(5)	7 077(5)
N(1)	10 000	5 000	9 701(3)
O(1)	9 269(3)	4 269(3)	10 176(3)
N(11)	10 000	5 000	6 708(3)
C(12)	9 132(3)	4 132(3)	6 226(3)
C(13)	9 102(4)	4 102(4)	5 206(3)
C(14)	10 000	5 000	4 710(3)
N(21)	8 503(3)	3 503(3)	7 877(2)
N(22)	8 337(2)	3 337(2)	6 865(2)
C(23)	7 336(4)	2 336(4)	6 704(5)
C(24)	6 885(4)	1 885(4)	7 574(4)
Cl(1c)	10 000	10 000	5 000
O(1c)	10 542(20)	10 386(35)	4 015(16)
O(2c)	8 799(9)	10 577(9)	4 793(8)

Table 5 Atomic coordinates ($\times 10^4$) for *trans*-$[Ru(bdmpp)(NO_2)(PMe_3)_2]ClO_4 \cdot H_2O$ **16**·H_2O

Atom	*x*	*y*	*z*
Ru	2 499(1)	9 444(1)	1 537(1)
P(1)	4 153(2)	8 384(2)	1 986(1)
C(1)	5 858(8)	9 234(9)	2 054(3)
C(2)	4 719(10)	6 684(8)	1 843(3)
C(3)	3 574(9)	8 118(10)	2 499(2)
P(2)	807(2)	10 455(2)	1 097(1)
C(4)	156(8)	9 329(9)	697(2)
C(5)	−872(8)	11 018(8)	1 338(3)
C(6)	1 440(8)	11 933(7)	815(2)
N(1)	2 450(7)	11 145(5)	1 919(1)
O(1)	3 165(5)	11 178(5)	2 239(2)
O(2)	1 738(7)	12 178(5)	1 835(2)
N(11)	2 610(6)	7 827(4)	1 172(1)
C(12)	1 731(7)	6 784(6)	1 228(2)
C(13)	1 799(9)	5 627(8)	992(2)
C(14)	2 844(9)	5 606(9)	697(2)
C(15)	3 770(8)	6 675(9)	633(2)
C(16)	3 609(7)	7 806(7)	874(2)
N(21)	880(5)	8 225(5)	1 764(2)
N(22)	744(6)	6 992(5)	1 555(1)
C(23)	−334(7)	6 228(7)	1 714(2)
C(24)	−897(7)	6 973(6)	2 023(2)
C(25)	−113(7)	8 206(7)	2 050(2)
C(26)	−770(10)	4 852(7)	1 574(2)
C(27)	−319(7)	9 322(8)	2 342(2)
N(31)	4 143(6)	10 012(6)	1 152(2)
N(32)	4 404(6)	8 998(6)	864(2)
C(33)	5 457(7)	9 461(10)	591(2)
C(34)	5 811(8)	10 728(8)	717(2)
C(35)	5 006(8)	11 036(7)	1 057(2)
C(36)	6 008(10)	8 685(11)	238(2)
C(37)	5 019(9)	12 311(8)	1 304(2)
Cl(1)	2 668(3)	171(3)	9 572(1)
O(1s)	2 612(15)	−338(14)	9 950(3)
O(2s)	2 894(20)	−954(13)	9 321(4)
O(3s)	1 375(15)	590(18)	9 535(7)
O(4s)	3 631(17)	1 052(13)	9 486(4)
O(1x)	3 851(13)	3 330(11)	10 046(3)

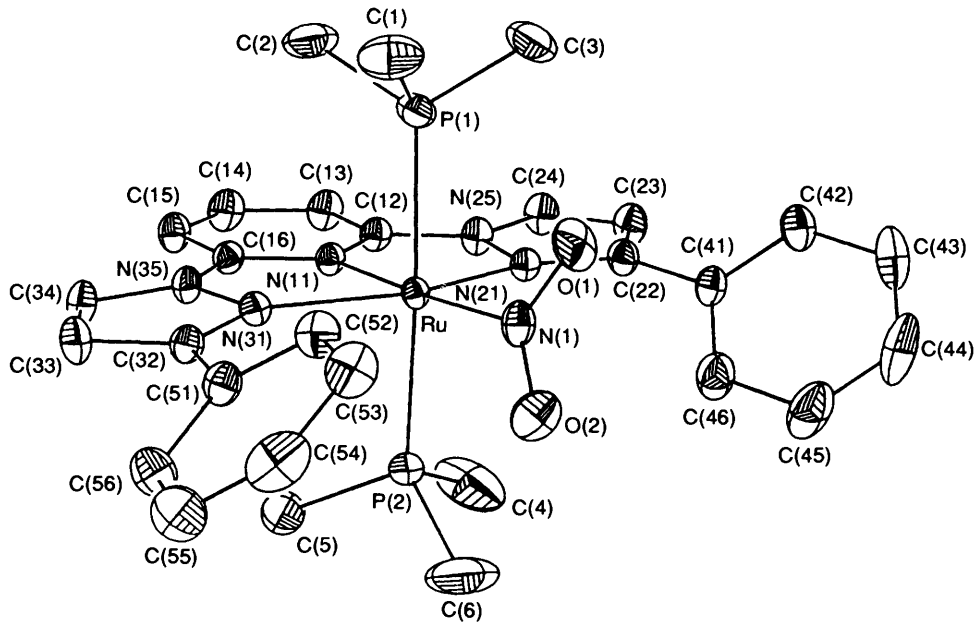

Fig. 4 An ORTEP II view of $[Ru(bppp)(NO_2)(PMe_3)_2]ClO_4$ **17**

Table 6 Atomic coordinates ($\times 10^4$) for *trans*-$[Ru(bppp)(NO_2)(PMe_3)_2]ClO_4$ **17**

Atom	*x*	*y*	*z*	Atom	*x*	*y*	*z*
Ru	1178(1)	1556(1)	2802(1)	N(35)	−491(3)	575(1)	2488(2)
P(1)	−464(1)	1921(1)	3792(1)	C(41)	2852(4)	3032(2)	2571(3)
C(1)	−455(6)	1713(3)	5009(4)	C(42)	2848(6)	3576(2)	2888(4)
C(2)	−2193(5)	1718(3)	3421(5)	C(43)	3994(8)	3804(3)	3324(4)
C(3)	−579(7)	2662(2)	3838(5)	C(44)	5125(8)	3506(3)	3429(5)
P(2)	2716(1)	1167(1)	1771(1)	C(45)	5146(6)	2965(3)	3150(5)
C(4)	2901(10)	1588(3)	752(5)	C(46)	4005(5)	2726(2)	2727(4)
C(5)	2220(7)	536(3)	1239(5)	C(51)	1903(4)	225(2)	4384(3)
C(6)	4424(6)	1070(4)	2073(7)	C(52)	2219(5)	657(2)	4992(3)
N(1)	2658(3)	1746(1)	3817(2)	C(53)	3145(5)	586(2)	5743(3)
O(1)	2399(3)	2096(2)	4431(2)	C(54)	3732(5)	69(3)	5888(4)
O(2)	3796(3)	1550(2)	3868(3)	C(55)	3442(6)	−359(2)	5284(4)
N(11)	−301(3)	1425(1)	1824(2)	C(56)	2530(5)	−287(2)	4538(3)
C(12)	−671(4)	1830(2)	1221(3)	Cl(1)	−726(1)	4309(1)	3566(1)
C(13)	−1714(4)	1769(2)	559(3)	O(1pa)	−34(17)	3876(7)	4033(13)
C(14)	−2392(5)	1264(2)	536(3)	O(1pb)	130(19)	4348(10)	4462(13)
C(15)	−2047(4)	846(2)	1160(3)	O(1pc)	−62(8)	4067(4)	4337(6)
C(16)	−983(4)	944(2)	1798(3)	O(2pa)	−610(31)	4891(14)	4127(24)
N(21)	1145(3)	2313(1)	2060(2)	O(2pb)	−1441(17)	4739(7)	3636(11)
C(22)	1672(4)	2827(2)	2013(3)	O(2pc)	−2129(11)	4439(5)	3939(7)
C(23)	958(5)	3139(2)	1315(3)	O(2pd)	−2080(18)	4136(8)	3474(13)
C(24)	9(5)	2807(2)	923(3)	O(2pe)	−1494(14)	3873(5)	2978(9)
N(25)	104(3)	2307(1)	1369(2)	O(2pf)	−630(16)	3932(6)	2811(9)
N(31)	565(3)	733(1)	3114(2)	O(2pg)	143(16)	4307(7)	2724(11)
C(32)	853(4)	271(2)	3621(3)	O(2ph)	277(16)	4598(7)	3043(12)
C(33)	−7(5)	−165(2)	3313(3)	O(2pj)	−733(12)	4874(5)	3254(8)
C(34)	−830(4)	33(2)	2613(3)				

trans-$[Ru(bppp)(NO_2)(PMe_3)_2]ClO_4$ **17**. Interatomic distances and angles are given in Table 10 and the molecule is illustrated in Fig. 4. This crystal consists of an array of $[Ru(bppp)(NO_2)(PMe_3)_2]^+$ cations and ClO_4^- anions in a 1 : 1 stoichiometry. The Ru–N(nitro) bond distance of 2.057(3) Å, the N(1)–O(1) bond distance of 1.255(5) Å and N(1)–O(2) bond distance of 1.224(5) Å, with an O(1)–N(1)–O(2) angle of 116.3(3)° are all within the range normally found for transition-metal nitro complexes.[15] The two Ru–N–O angles have significantly different values, with Ru–N(1)–O(1) 118.4(3) and Ru–N(1)–O(2) 125.3(3)°. The plane of the nitro ligand is oriented at 70.6° to the meridional co-ordination plane of the bppp ligand, with the nitrogen atom of the nitro group lying 0.100 Å from the meridional co-ordination plane. The *trans*-phosphine ligand arrangement was confirmed with the P(1)–Ru–P(2) angle being 176.9(1)° and Ru–P bond distances of 2.389(1) and 2.377(1) Å, each within the range reported for other ruthenium complexes.[47–51] The bppp ligand is bound to the three remaining co-ordination sites in a meridional fashion through three of its nitrogen atoms. The central pyridine fragment of bppp is bound *trans* to the nitro ligand, with a N(11)–Ru–N(1) angle of 176.1(1)°. The N–Ru–N angles between the nitrogen atom of the pyridine fragment [N(11)] and the pyrazole fragments [N(21) and N(22)] show the usual distortions due to the geometric constraints of the terdentate ligand, with N(11)–Ru–N(21) 78.1(1) and N(11)–Ru–N(31)

Table 7 Atomic coordinates ($\times 10^4$) for *trans*-[Ru(bcppp)(NO_2)(PMe_3)$_2$]ClO_4·0.5H_2O **18**·0.5H_2O

Atom	*x*	*y*	*z*	Atom	*x*	*y*	*z*
Ru(1a)	5 000	2 340(1)	5 000	C(4b)	9 872(9)	−136(11)	745(5)
Ru(1b)	10 230(1)	3 016(1)	1 310(1)	C(5b)	8 304(7)	979(14)	1 135(5)
P(1a)	5 711(1)	701(2)	4 458(1)	C(6b)	8 948(6)	1 816(10)	82(3)
C(1a)	5 993(7)	1 287(11)	3 767(4)	N(1b)	9 261(4)	4 403(7)	1 179(2)
C(2a)	6 783(6)	227(12)	4 772(4)	O(1b)	9 339(4)	5 552(5)	1 348(2)
C(3a)	5 218(8)	−851(10)	4 261(6)	O(2b)	8 535(3)	4 101(6)	931(3)
P(2a)	4 327(2)	3 997(3)	5 537(1)	N(11b)	11 186(4)	1 691(6)	1 463(3)
C(4a)	3 263(8)	4 535(14)	5 303(5)	C(12b)	11 193(5)	959(7)	1 932(3)
C(5a)	4 816(13)	5 525(13)	5 543(10)	C(13b)	11 854(7)	64(10)	2 077(5)
C(6a)	4 230(10)	3 702(19)	6 286(4)	C(14b)	12 493(6)	−78(11)	1 693(5)
N(1a)	4 049(4)	1 074(7)	5 260(3)	C(15b)	12 491(6)	620(10)	1 192(5)
O(1a)	4 022(4)	−129(7)	5 165(3)	C(16b)	11 814(5)	1 524(8)	1 093(3)
O(2a)	3 425(6)	1 482(9)	5 484(5)	N(21b)	9 872(4)	2 152(6)	2 085(3)
N(11a)	5 886(4)	3 644(6)	4 756(2)	C(22b)	9 219(5)	2 044(7)	2 451(3)
C(12a)	5 706(5)	4 375(7)	4 278(3)	C(23b)	9 422(6)	1 052(9)	2 851(4)
C(13a)	6 256(6)	5 317(8)	4 105(4)	C(24b)	10 201(6)	558(9)	2 727(4)
C(14a)	7 027(6)	5 544(9)	4 438(4)	N(25b)	10 484(4)	1 212(6)	2 271(3)
C(15a)	7 238(5)	4 810(8)	4 937(3)	N(31b)	10 982(4)	3 185(6)	564(3)
C(16a)	6 629(4)	3 866(7)	5 072(3)	C(32b)	10 974(5)	3 662(8)	32(3)
N(21a)	4 361(4)	3 125(6)	4 255(3)	C(33b)	11 676(5)	3 132(8)	−259(4)
C(22a)	3 596(5)	3 191(7)	3 934(3)	C(34b)	12 125(6)	2 311(10)	118(4)
C(23a)	3 625(6)	4 200(9)	3 528(4)	N(35b)	11 684(4)	2 324(6)	611(3)
C(24a)	4 422(6)	4 739(9)	3 574(3)	C(41b)	8 424(5)	2 825(8)	2 429(3)
N(25a)	4 893(4)	4 083(6)	4 015(3)	C(42b)	8 414(5)	4 182(8)	2 377(3)
N(31a)	6 001(4)	2 224(6)	5 672(3)	C(43b)	7 637(6)	4 867(10)	2 369(4)
C(32a)	6 219(5)	1 704(7)	6 181(3)	C(44b)	6 858(6)	4 225(12)	2 412(4)
C(33a)	7 047(5)	2 207(8)	6 399(3)	C(45b)	6 849(6)	2 888(12)	2 474(4)
C(34a)	7 303(5)	3 079(9)	6 004(3)	C(46b)	7 625(6)	2 172(10)	2 477(4)
N(35a)	6 685(4)	3 077(6)	5 562(2)	Cl(4b)	5 881(2)	5 092(4)	2 408(2)
C(41a)	2 838(5)	2 350(9)	4 018(3)	C(51b)	10 327(5)	4 593(8)	−206(3)
C(42a)	2 882(6)	999(10)	4 035(4)	C(52b)	10 046(6)	5 640(8)	111(3)
C(43a)	2 148(6)	225(12)	4 078(4)	C(53b)	9 411(6)	6 491(10)	−128(4)
C(44a)	1 365(6)	815(13)	4 114(4)	C(54b)	9 087(6)	6 299(10)	−687(4)
C(45a)	1 296(7)	2 151(13)	4 096(5)	C(55b)	9 366(6)	5 318(10)	−1 009(4)
C(46a)	2 007(6)	2 919(11)	4 024(5)	C(56b)	9 983(7)	4 449(10)	−772(3)
Cl(4a)	423(2)	−143(4)	4 169(1)	Cl(5b)	8 309(2)	7 406(4)	−978(2)
C(51a)	5 690(5)	763(8)	6 482(3)	Cl(1a)	13 071(3)	7 594(3)	3 135(2)
C(52a)	5 335(6)	−352(8)	6 226(4)	O(1sa)	13 363(14)	6 749(12)	2 736(5)
C(53a)	4 835(6)	−1 198(10)	6 533(5)	O(2sa)	12 130(15)	7 540(23)	3 108(11)
C(54a)	4 721(6)	−942(9)	7 097(4)	O(3sa)	13 284(7)	8 927(9)	3 018(5)
C(55a)	5 059(7)	125(10)	7 357(4)	O(4sa)	13 258(9)	7 327(10)	3 703(5)
C(56a)	5 561(6)	991(9)	7 050(3)	Cl(1b)	7 823(2)	8 244(2)	3 282(1)
Cl(5a)	4 120(2)	−2 062(4)	7 481(2)	O(1sb)	7 858(8)	8 545(11)	2 719(4)
P(1b)	11 135(1)	4 600(2)	1 830(1)	O(2sb)	8 374(11)	7 319(15)	3 446(9)
C(1b)	11 380(7)	6 193(9)	1 501(5)	O(3sb)	7 003(9)	7 738(14)	3 365(6)
C(2b)	12 261(6)	4 029(11)	1 995(5)	O(4sb)	7 994(7)	9 391(11)	3 607(4)
C(3b)	10 824(7)	5 057(12)	2 528(4)	O(1s)	9 464(12)	8 071(15)	2 000(8)
P(2b)	9 333(1)	1 441(2)	813(1)				

78.0(1)°. Evidence of steric strain is further seen in the Ru–N bond lengths, where that to the central pyridine fragment [Ru–N(11) 1.995(3) Å] is substantially shorter than those to the peripheral pyrazole fragments [Ru–N(21) 2.109(3) and Ru–N(31) 2.127(3) Å].

An interesting feature of the *trans*-[Ru(bppp)(NO_2)(PMe_3)$_2$]ClO_4 structure is the angle that the phenyl rings make with the meridional co-ordination plane. Both of these rings are twisted in the same direction, a general orientation they share with the nitrite ligand. The O(1)–N(1)–O(2) angle is 116.3(3). The plane of the ring containing C(41) makes an angle of 47.3° with the meridional co-ordination plane, while that containing C(51) is angled at 38.0°, so although the angles are quite different, all three fragments are loosely oriented along the same general diagonal.

trans-[Ru(bcppp)(NO_2)(PMe_3)$_2$]ClO_4·0.5H_2O **18**·0.5H_2O. The crystal consists of an ordered array of *trans*-[Ru(bcppp)(NO_2)(PMe_3)$_2$]$^+$ cations, ClO_4^- anions and H_2O molecules of solvation in a 2:2:1 ratio. Interatomic distances and angles are collected in Table 11. The crystallographic asymmetric unit consists of two cations, two anions and an H_2O molecule (see Fig. 5). The cations are labelled as a and b. The b cations alone participate in hydrogen bonding to the single H_2O molecule of solvation, through atom O(2b) of its nitrite ligand. The following discussion will emphasize the a cation, which is illustrated in Fig. 6, the corresponding values for the b cation being cited in square brackets immediately following those for the a molecule. An exception to this will be for those values concerning hydrogen bonding to the nitro ligand in which only the b cation participates.

The two phosphine ligands of complex **18** lie almost directly *trans* to one another, with the P(1a)–Ru(1a)–P(2a) angle being 178.6(1) [179.0(1)°]. The observed Ru–P bond distances were 2.392(2) and 2.371(3) [2.402(2) and 2.364(2) Å], both within the range of 2.26–2.41 Å previously reported. The bcppp ligand is bound to the three remaining octahedral co-ordination sites in a meridional fashion through three of its nitrogen atoms. The central pyridine fragment of the terdentate ligand is bound to ruthenium in a location *trans* to the nitro ligand, with N(11a)–Ru(1a)–N(1a) 177.2(3) [178.1(2)°]. Steric strain is again evidenced in the N–Ru–N bond angles between the central pyridine nitrogen [N(11a)] and the terminal pyrazoles [N(21a)

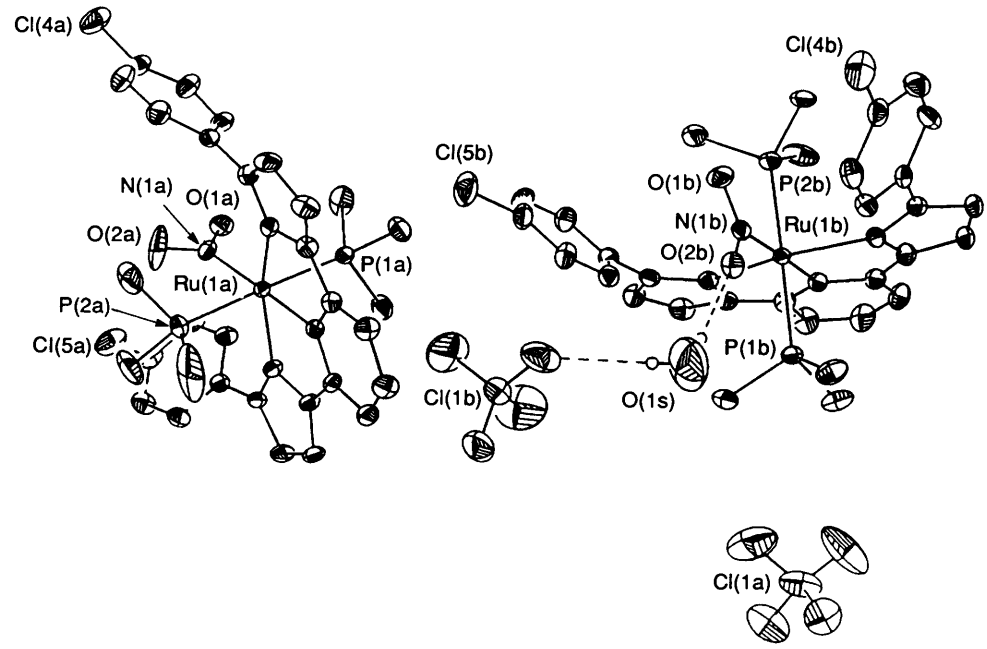

Fig. 5 The crystallographic asymmetric unit of $[Ru(bcppp)(NO_2)(PMe_3)_2]ClO_4 \cdot 0.5H_2O$ **18**·$0.5H_2O$

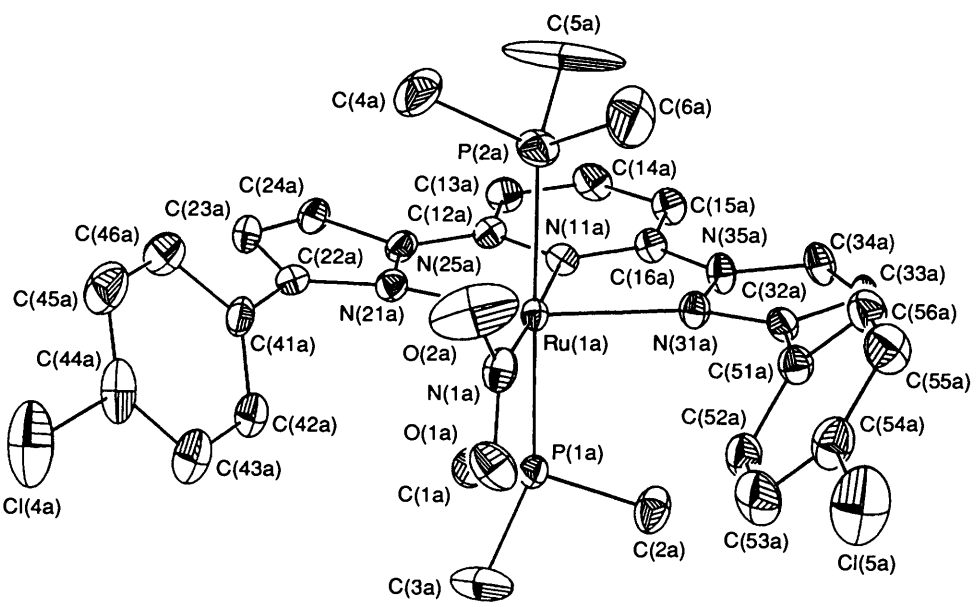

Fig. 6 An ORTEP II view of cation a of $[Ru(bcppp)(NO_2)(PMe_3)_2]^+$ in **18**

and N(31a)], angles of interest being 78.4(2)° for N(11a)–Ru(1a)–N(21a) and 77.3(2)° for N(11a)–Ru(1a)–N(31a) [77.9(2) and 77.3(2)°]. The Ru–N bond lengths again show distortion from ideal octahedral geometry, with the central Ru–N(pyridine) bond shorter at 2.001(6) [2.001(6) Å] than the terminal Ru–N bonds to the pyrazole fragments, which have values of 2.099(6) and 2.125(6) [2.113(6) and 2.151(6) Å]. The Ru(bcppp) moiety is not quite planar, with the ruthenium atom lying 0.086 (0.091 Å) from the meridional co-ordination plane of the bcppp ligand. The phenyl rings bonded to the bcppp ligand form opposing angles to the meridional co-ordination plane of the bcppp, with the angle for the plane of the ring containing C(41a) being 59.2 (55.5°) and that containing C(51a) being 53.0 (50.6°) from the meridional co-ordination plane.

The Ru–N(nitro) bond distances of 2.058(7) [2.052(6) Å] are not significantly different from one another. The hydrogen bonding in the b molecule, however, does effect the N–O bond distances. Interestingly, the N–O bond distances in the unperturbed molecule a are inequivalent with values of 1.244(10) Å for N(1a)–O(1a) and 1.189(12) Å for N(1a)–O(2a), whereas those in molecule b (where there is $NO_2 \cdots H_2O$ hydrogen bonding) are nearly equivalent with values of 1.237(8) and 1.256(8) Å. The average N–O distance in molecule b is, as expected, increased from that in a (1.247 *vs.* 1.217 Å) due to hydrogen bonding between the nitro group and the water molecule. The hydrogen-bonding distance O(1b)···O(1s) is 2.995 Å, while O(1b)···H(1s) is 2.234 Å. The O–N–O angles in the two molecules are also significantly different, with 113.7(7)° for O(1a)–N(1a)–O(2a) and 116.3(6)° for O(1b)–N(1b)–O(2b), each being within the 113–127° range.[29] The Ru–N–O bond angles are 125.4(5)° for Ru(1a)–N(1a)–O(1a), 120.6(7)° for Ru(1a)–N(1a)–O(2a), 123.2(4)° for Ru(1b)–N(1b)–O(1b) and 120.5(5)° for Ru(1b)–N(1b)–O(2b). The plane of the nitro ligand is also affected by hydrogen bonding. The nitro ligand in molecule a is oriented at an angle of 81.4° to the meridional co-ordination plane of the bcppp ligand, with the nitrogen atom

0.08 Å from the meridional co-ordination plane. The nitro ligand in the hydrogen-bonded molecule b is oriented at an angle of 88.0°, with the nitrogen atom now being displaced by 0.24 Å.

Additional Comments.—The effects of steric crowding in the vicinity of the nitrite ligand manifest themselves in the lengthening of the adjacent Ru–N(pyrazole) bonds and the twisting of the nitrite plane relative to the meridional co-ordination plane. As steric crowding about the nitrite ligand increases, we observe that in addition to the nitro ligand displacement from the RuL plane the Ru–N(pyrazole) bond distances increase. It appears as if the terdentate ligand were being 'wedged open' by the nitrite group. Indeed, while the Ru–N(pyrazole) distances for complexes **17** [2.109(3) and 2.127(3) Å] and **18** [2.099(6) and 2.125(6) Å] are similar to each other, they are significantly longer than the analogous distances for **15** [2.070(3) Å] and **16** [2.071(5) and 2.068(6) Å], which have a less-crowded nitrite position.

A more sensitive indicator of steric crowding around the nitrite ligand is the orientation of the O–N–O plane relative to the meridional co-ordination plane. Since there should be essentially free rotation about the Ru–N(NO_2) bond, the O–N–O plane should be oriented so as to minimize steric strain in the solid state. In complex **15** the O–N–O plane is contained within the meridional co-ordination plane, while for **16**–**18** it is close to perpendicular to the meridional plane. We have defined the twist angle as the acute angle between the O–N–O plane of the nitrite ligand and the meridional co-ordination plane. The twist angles are as follows: 0.0, **15**; 88.8, **16**; 70.6, **17**; and 81.2°, **18**. These observations lend support to the mechanisms postulated by Muidaka[32] and Meyer[41] and co-workers for the decomposition of nitroruthenium(III) complexes where they suggest that the nitro ligand isomerizes to the *O*-bound nitrito form.

From our structural studies we can now contrast the steric properties of bpp with one of the most often studied terdentate ligands, terpy. The Ru–N(terminal pyridine) bond lengths of 2.088(6) and 2.093(7) Å for the $[Ru(terpy)(PMe_3)_2(NO_2)]^+$ complex are slightly longer than the Ru–N(terminal pyrazole) bond lengths of 2.070(3) Å in **15**. Also, although the N atom of the nitro ligand was not displaced from the RuL in either complex, the nitro ligand in the $[Ru(terpy)(PMe_3)_2(NO_2)]^+$ complex is twisted slightly (19.8°) out of the Ru(terpy) plane while that of **15** is contained within the Ru(bpp) plane. Thus, we propose that bpp may be slightly sterically smaller than terpy because the latter causes a lengthening of the Ru–N(terminal pyridine or pyrazole) bond length and a twisting of the N–O vectors of the nitro ligand from the RuL plane.

Table 8 Interatomic distances (Å) and angles (°) with e.s.d.s for complex **15**

Ru–N(1)	2.058(4)	Ru–N(11)	1.990(3)
Ru–N(21)	2.070(3)	Ru–P(1)	2.360(1)
P(1)–C(1)	1.812(4)	P(1)–C(2)	1.798(6)
N(1)–O(1)	1.182(4)	N(11)–C(12)	1.346(4)
C(12)–C(13)	1.380(6)	C(12)–N(22)	1.381(5)
C(13)–C(14)	1.391(6)	N(21)–N(22)	1.387(4)
N(21)–C(25)	1.322(5)	N(22)–C(23)	1.374(6)
C(23)–C(24)	1.326(8)	C(24)–C(25)	1.384(7)
N(1)–Ru–N(11)	180.0(—)	N(1)–Ru–N(21)	101.4(1)
N(11)–Ru–N(21)	78.6(1)	N(1)–Ru–P(1)	88.0(1)
N(11)–Ru–P(1)	92.0(1)	N(21)–Ru–P(1)	90.4(1)
P(1)–Ru–P(1a)	176.0(1)	N(21)–Ru–N(21a)	157.2(2)
C(1)–P(1)–C(2)	103.2(2)	C(1)–P(1)–Ru	114.0(1)
C(2)–P(1)–Ru	116.9(1)	Ru–N(1)–O(1)	122.9(2)
O(1)–N(1)–O(1a)	114.1(5)	Ru–N(11)–C(12)	119.0(2)
C(12)–N(11)–C(12a)	122.0(4)	N(11)–C(12)–C(13)	120.7(4)
N(11)–C(12)–N(22)	112.3(3)	C(13)–C(12)–N(22)	127.0(4)
C(12)–C(13)–C(14)	117.1(4)	C(13)–C(14)–C(13a)	122.4(5)
Ru–N(21)–N(22)	110.8(2)	Ru–N(21)–C(25)	143.9(3)
N(22)–N(21)–C(25)	105.4(3)	C(12)–N(22)–N(21)	119.4(3)
C(12)–N(22)–C(23)	132.2(4)	N(21)–N(22)–C(23)	108.4(4)
N(22)–C(23)–C(24)	108.4(5)	C(23)–C(24)–C(25)	106.6(5)
N(21)–C(25)–C(24)	111.2(4)		

Acknowledgements

We gratefully acknowledge the National Science Foundation (CHE 9120602) (K. J. T.), the Donors of the Petroleum Research Fund administered by the American Chemical Society (D. L. J.), the Whitaker Foundation of Research Corporation (D. L. J.), Gettysburg College through an Institutional Self Renewal Grant (D. L. J.), and ARCO Chemical Corporation

Table 9 Interatomic distances (Å) and angles (°) with e.s.d.s for complex **16**·H_2O

Ru–P(1)	2.378(2)	Ru–P(2)	2.364(2)	C(13)–C(14)	1.378(11)	C(14)–C(15)	1.377(12)
Ru–N(1)	2.087(5)	Ru–N(11)	1.992(4)	C(15)–C(16)	1.370(10)	C(16)–N(32)	1.386(9)
Ru–N(21)	2.071(5)	Ru–N(31)	2.068(6)	N(21)–N(22)	1.396(7)	N(21)–C(25)	1.321(8)
P(1)–C(1)	1.816(8)	P(1)–C(2)	1.810(8)	N(22)–C(23)	1.361(8)	C(23)–C(24)	1.356(9)
P(1)–C(3)	1.791(8)	P(2)–C(4)	1.821(8)	C(23)–C(26)	1.484(10)	C(24)–C(25)	1.418(9)
P(2)–C(5)	1.846(8)	P(2)–C(6)	1.819(8)	C(25)–C(27)	1.468(10)	N(31)–N(32)	1.395(8)
N(1)–O(1)	1.247(7)	N(1)–O(2)	1.243(8)	N(31)–C(35)	1.327(9)	N(32)–C(33)	1.408(9)
N(11)–C(12)	1.326(8)	N(11)–C(16)	1.355(8)	C(33)–C(34)	1.351(12)	C(33)–C(36)	1.480(12)
C(12)–C(13)	1.375(9)	C(12)–N(22)	1.433(8)	C(34)–C(35)	1.381(10)	C(35)–C(37)	1.489(11)
P(1)–Ru–P(2)	178.4(1)	P(1)–Ru–N(1)	89.5(2)	N(11)–C(12)–N(22)	113.3(5)	C(13)–C(12)–N(22)	124.8(6)
P(2)–Ru–N(1)	91.0(2)	P(1)–Ru–N(11)	89.5(1)	C(12)–C(13)–C(14)	116.2(7)	C(13)–C(14)–C(15)	122.9(7)
P(2)–Ru–N(11)	90.0(2)	N(1)–Ru–N(11)	178.3(2)	C(14)–C(15)–C(16)	117.3(7)	N(11)–C(16)–C(15)	120.3(6)
P(1)–Ru–N(21)	90.1(1)	P(2)–Ru–N(21)	88.3(1)	N(11)–C(16)–N(32)	112.1(5)	C(15)–C(16)–N(32)	127.5(6)
N(1)–Ru–N(21)	103.2(2)	N(11)–Ru–N(21)	78.2(2)	Ru–N(21)–N(22)	112.9(3)	Ru–N(21)–C(25)	141.2(4)
P(1)–Ru–N(31)	90.7(2)	P(2)–Ru–N(31)	90.7(2)	N(22)–N(21)–C(25)	105.9(5)	C(12)–N(22)–N(21)	115.7(5)
N(1)–Ru–N(31)	99.7(2)	N(11)–Ru–N(31)	78.9(2)	C(12)–N(22)–C(23)	133.5(5)	N(21)–N(22)–C(23)	110.8(5)
N(21)–Ru–N(31)	157.0(2)	Ru–P(1)–C(1)	116.7(3)	N(22)–C(23)–C(24)	106.3(6)	N(22)–C(23)–C(26)	125.8(6)
Ru–P(1)–C(2)	115.7(3)	C(1)–P(1)–C(2)	101.3(4)	C(24)–C(23)–C(26)	128.0(6)	C(23)–C(24)–C(25)	107.7(6)
Ru–P(1)–C(3)	116.7(3)	C(1)–P(1)–C(3)	102.5(4)	N(21)–C(25)–C(24)	109.4(5)	N(21)–C(25)–C(27)	123.2(6)
C(2)–P(1)–C(3)	101.5(4)	Ru–P(2)–C(4)	114.4(3)	C(24)–C(25)–C(27)	127.5(6)	Ru–N(31)–N(32)	110.8(4)
Ru–P(2)–C(5)	115.7(3)	C(4)–P(2)–C(5)	101.9(4)	Ru–N(31)–C(35)	143.3(5)	N(32)–N(31)–C(35)	105.8(6)
Ru–P(2)–C(6)	115.2(3)	C(4)–P(2)–C(6)	103.0(4)	C(16)–N(32)–N(31)	119.4(5)	C(16)–N(32)–C(33)	131.5(6)
C(5)–P(2)–C(6)	105.0(4)	Ru–N(1)–O(1)	121.0(4)	N(31)–N(32)–C(33)	109.0(6)	N(32)–C(33)–C(34)	105.8(6)
Ru–N(1)–O(2)	121.9(4)	O(1)–N(1)–O(2)	117.0(5)	N(32)–C(33)–C(36)	125.3(8)	C(34)–C(33)–C(36)	128.9(7)
Ru–N(11)–C(12)	119.9(4)	Ru–N(11)–C(16)	118.9(4)	C(33)–C(34)–C(35)	108.4(7)	N(31)–C(35)–C(34)	111.0(7)
C(12)–N(11)–C(16)	121.2(5)	N(11)–C(12)–C(13)	121.9(6)	N(31)–C(35)–C(37)	120.8(6)	C(34)–C(35)–C(37)	128.3(7)

Table 10 Interatomic distances (Å) and angles (°) with e.s.d.s for complex **17**

Ru–P(1)	2.389(1)	Ru–P(2)	2.377(1)	C(22)–C(23)	1.407(6)	C(22)–C(41)	1.466(5)
Ru–N(1)	2.057(3)	Ru–N(11)	1.995(3)	C(23)–C(24)	1.335(6)	C(24)–N(25)	1.363(5)
Ru–N(21)	2.109(3)	Ru–N(31)	2.127(3)	N(31)–C(32)	1.350(5)	N(31)–N(35)	1.392(4)
P(1)–C(1)	1.811(6)	P(1)–C(2)	1.836(5)	C(32)–C(33)	1.409(6)	C(32)–C(51)	1.470(5)
P(1)–C(3)	1.789(5)	P(2)–C(4)	1.794(8)	C(33)–C(34)	1.344(6)	C(34)–N(35)	1.362(5)
P(2)–C(5)	1.757(7)	P(2)–C(6)	1.744(6)	C(41)–C(42)	1.385(6)	C(41)–C(46)	1.370(6)
N(1)–O(1)	1.255(5)	N(1)–O(2)	1.224(5)	C(42)–C(43)	1.381(9)	C(43)–C(44)	1.335(11)
N(11)–C(12)	1.338(5)	N(11)–C(16)	1.341(5)	C(44)–C(45)	1.363(11)	C(45)–C(46)	1.380(8)
C(12)–C(13)	1.371(5)	C(12)–N(25)	1.392(5)	C(51)–C(52)	1.380(6)	C(51)–C(56)	1.392(6)
C(13)–C(14)	1.390(7)	C(14)–C(15)	1.375(6)	C(52)–C(53)	1.384(6)	C(53)–C(54)	1.387(9)
C(15)–C(16)	1.377(5)	C(16)–N(35)	1.395(5)	C(54)–C(55)	1.364(9)	C(55)–C(56)	1.371(7)
N(21)–C(22)	1.347(5)	N(21)–N(25)	1.390(4)				
P(1)–Ru–P(2)	176.9(1)	P(1)–Ru–N(1)	89.2(1)	N(11)–C(16)–N(35)	112.0(3)	C(15)–C(16)–N(35)	125.8(4)
P(2)–Ru–N(1)	93.8(1)	P(1)–Ru–N(11)	88.4(1)	Ru–N(21)–C(22)	145.6(2)	Ru–N(21)–N(25)	109.7(2)
P(2)–Ru–N(11)	88.7(1)	N(1)–Ru–N(11)	176.1(1)	C(22)–N(21)–N(25)	104.5(3)	N(21)–C(22)–C(23)	110.1(3)
P(1)–Ru–N(21)	89.4(1)	P(2)–Ru–N(21)	91.2(1)	N(21)–C(22)–C(41)	125.6(3)	C(23)–C(22)–C(41)	124.2(4)
N(1)–Ru–N(21)	98.8(1)	N(11)–Ru–N(21)	78.1(1)	C(22)–C(23)–C(24)	107.1(4)	C(23)–C(24)–N(25)	107.7(4)
P(1)–Ru–N(31)	90.2(1)	P(2)–Ru–N(31)	88.0(1)	C(12)–N(25)–N(21)	120.0(3)	C(12)–N(25)–C(24)	129.4(3)
N(1)–Ru–N(31)	105.1(1)	N(11)–Ru–N(31)	78.0(1)	N(21)–N(25)–C(24)	110.6(3)	Ru–N(31)–C(32)	145.6(2)
N(21)–Ru–N(31)	156.1(1)	Ru–P(1)–C(1)	120.1(2)	Ru–N(31)–N(35)	109.5(2)	C(32)–N(31)–N(35)	104.4(3)
Ru–P(1)–C(2)	113.0(2)	C(1)–P(1)–C(2)	99.0(3)	N(31)–C(32)–C(33)	109.9(3)	N(31)–C(32)–C(51)	125.5(3)
Ru–P(1)–C(3)	115.8(2)	C(1)–P(1)–C(3)	103.7(3)	C(33)–C(32)–C(51)	124.6(4)	C(32)–C(33)–C(34)	107.5(4)
C(2)–P(1)–C(3)	102.5(3)	Ru–P(2)–C(4)	112.4(3)	C(33)–C(34)–N(35)	107.0(4)	C(16)–N(35)–N(31)	120.1(3)
Ru–P(2)–C(5)	115.8(2)	C(4)–P(2)–C(5)	100.1(3)	C(16)–N(35)–C(34)	128.5(3)	N(31)–N(35)–C(34)	111.2(3)
Ru–P(2)–C(6)	123.5(3)	C(4)–P(2)–C(6)	97.6(5)	C(22)–C(41)–C(42)	118.6(4)	C(22)–C(41)–C(46)	122.9(4)
C(5)–P(2)–C(6)	103.7(4)	Ru–N(1)–O(1)	118.4(3)	C(42)–C(41)–C(46)	118.3(4)	C(41)–C(42)–C(43)	120.4(5)
Ru–N(1)–O(2)	125.3(3)	O(1)–N(1)–O(2)	116.3(3)	C(42)–C(43)–C(44)	120.3(6)	C(43)–C(44)–C(45)	120.5(7)
Ru–N(11)–C(12)	120.1(2)	Ru–N(11)–C(16)	120.4(2)	C(44)–C(45)–C(46)	120.1(6)	C(41)–C(46)–C(45)	120.3(5)
C(12)–N(11)–C(16)	119.4(3)	N(11)–C(12)–C(13)	122.4(4)	C(32)–C(51)–C(52)	122.4(4)	C(32)–C(51)–C(56)	118.4(4)
N(11)–C(12)–N(25)	111.9(3)	C(13)–C(12)–N(25)	125.6(4)	C(52)–C(51)–C(56)	119.0(4)	C(51)–C(52)–C(53)	120.9(4)
C(12)–C(13)–C(14)	117.2(4)	C(13)–C(14)–C(15)	121.5(4)	C(52)–C(53)–C(54)	118.8(5)	C(53)–C(54)–C(55)	120.8(5)
C(14)–C(15)–C(16)	117.3(4)	N(11)–C(16)–C(15)	122.3(4)	C(54)–C(55)–C(56)	120.2(5)	C(51)–C(56)–C(55)	120.3(4)

Table 11 Interatomic distances (Å) and angles (°) with e.s.d.s for complex **18**·0.5H_2O

Ru(1a)–P(1a)	2.392(2)	Ru(1a)–P(2a)	2.371(3)	C(51a)–C(56a)	1.373(11)	C(52a)–C(53a)	1.379(13)
Ru(1a)–N(1a)	2.058(7)	Ru(1a)–N(11a)	2.001(6)	C(53a)–C(54a)	1.364(15)	C(54a)–C(55a)	1.332(13)
Ru(1a)–N(21a)	2.099(6)	Ru(1a)–N(31a)	2.125(6)	C(54a)–Cl(5a)	1.743(10)	C(55a)–C(56a)	1.393(13)
Ru(1b)–P(1b)	2.402(2)	Ru(1b)–P(2b)	2.364(2)	P(1b)–C(1b)	1.841(10)	P(1b)–C(2b)	1.831(10)
Ru(1b)–N(1b)	2.052(6)	Ru(1b)–N(11b)	2.001(6)	P(1b)–C(3b)	1.787(10)	P(2b)–C(4b)	1.814(12)
Ru(1b)–N(21b)	2.113(6)	Ru(1b)–N(31b)	2.151(6)	P(2b)–C(5b)	1.841(12)	P(2b)–C(6b)	1.814(9)
P(1a)–C(1a)	1.797(9)	P(1a)–C(2a)	1.815(10)	N(1b)–O(1b)	1.237(8)	N(1b)–O(2b)	1.256(8)
P(1a)–C(3a)	1.796(11)	P(2a)–C(4a)	1.767(12)	N(11b)–C(12b)	1.324(10)	N(11b)–C(16b)	1.340(10)
P(2a)–C(5a)	1.723(15)	P(2a)–C(6a)	1.791(11)	C(12b)–C(13b)	1.384(12)	C(12b)–N(25b)	1.403(10)
N(1a)–O(1a)	1.244(10)	N(1a)–O(2a)	1.189(12)	C(13b)–C(14b)	1.371(15)	C(14b)–C(15b)	1.369(16)
N(11a)–C(12a)	1.355(9)	N(11a)–C(16a)	1.332(9)	C(15b)–C(16b)	1.392(12)	C(16b)–N(35b)	1.393(11)
C(12a)–C(13a)	1.351(11)	C(12a)–N(25a)	1.382(9)	N(21b)–C(22b)	1.356(10)	N(21b)–N(25b)	1.387(8)
C(13a)–C(14a)	1.387(12)	C(14a)–C(15a)	1.405(12)	C(22b)–C(23b)	1.397(11)	C(22b)–C(41b)	1.447(11)
C(15a)–C(16a)	1.386(11)	C(16a)–N(35a)	1.397(9)	C(23b)–C(24b)	1.337(13)	C(24b)–N(25b)	1.350(11)
N(21a)–C(22a)	1.350(9)	N(21a)–N(25a)	1.407(8)	N(31b)–C(32b)	1.334(9)	N(31b)–N(35b)	1.381(9)
C(22a)–C(23a)	1.399(11)	C(22a)–C(41a)	1.460(11)	C(32b)–C(33b)	1.409(11)	C(32b)–C(51b)	1.453(10)
C(23a)–C(24a)	1.331(13)	C(24a)–N(25a)	1.390(10)	C(33b)–C(34b)	1.366(12)	C(34b)–N(35b)	1.368(11)
N(31a)–C(32a)	1.324(9)	N(31a)–N(35a)	1.392(8)	C(41b)–C(42b)	1.385(12)	C(41b)–C(46b)	1.397(13)
C(32a)–C(33a)	1.427(10)	C(32a)–C(51a)	1.460(10)	C(42b)–C(43b)	1.373(12)	C(43b)–C(44b)	1.364(13)
C(33a)–C(34a)	1.353(12)	C(34a)–C(35a)	1.356(9)	C(44b)–C(45b)	1.368(17)	C(44b)–Cl(4b)	1.731(10)
C(41a)–C(42a)	1.376(13)	C(41a)–C(46a)	1.394(12)	C(45b)–C(46b)	1.389(14)	C(51b)–C(52b)	1.380(11)
C(42a)–C(43a)	1.376(13)	C(43a)–C(44a)	1.343(14)	C(51b)–C(56b)	1.400(11)	C(52b)–C(53b)	1.390(12)
C(44a)–C(45a)	1.363(19)	C(44a)–Cl(4a)	1.747(11)	C(53b)–C(54b)	1.383(13)	C(54b)–C(55b)	1.334(14)
C(45a)–C(46a)	1.356(15)	C(51a)–C(52a)	1.376(11)	C(54b)–Cl(5b)	1.743(10)	C(55b)–C(56b)	1.380(13)
P(1a)–Ru(1a)–P(2a)	178.6(1)	P(1a)–Ru(1a)–N(1a)	94.1(2)	C(43a)–C(44a)–C(45a)	120.7(10)	C(43a)–C(44a)–Cl(4a)	119.6(10)
P(2a)–Ru(1a)–N(1a)	87.3(2)	P(1a)–Ru(1a)–N(11a)	88.6(2)	C(45a)–C(44a)–Cl(4a)	119.7(8)	C(44a)–C(45a)–C(46a)	121.1(10)
P(2a)–Ru(1a)–N(11a)	90.1(2)	N(1a)–Ru(1a)–N(11a)	177.2(3)	C(41a)–C(46a)–C(45a)	119.8(10)	C(32a)–C(51a)–C(52a)	123.0(7)
P(1a)–Ru(1a)–N(21a)	91.7(2)	P(2a)–Ru(1a)–N(21a)	88.5(2)	C(32a)–C(51a)–C(56a)	118.1(7)	C(52a)–C(51a)–C(56a)	118.9(8)
N(1a)–Ru(1a)–N(21a)	100.5(2)	N(11a)–Ru(1a)–N(21a)	78.4(2)	C(51a)–C(52a)–C(53a)	120.2(8)	C(52a)–C(53a)–C(54a)	119.4(9)
P(1a)–Ru(1a)–N(31a)	91.4(2)	P(2a)–Ru(1a)–N(31a)	87.9(2)	C(53a)–C(54a)–C(55a)	121.7(9)	C(53a)–C(54a)–Cl(5a)	118.3(7)
N(1a)–Ru(1a)–N(31a)	103.5(2)	N(11a)–Ru(1a)–N(31a)	77.3(2)	C(55a)–C(54a)–Cl(5a)	120.0(8)	C(54a)–C(55a)–C(56a)	119.3(8)
N(21a)–Ru(1a)–N(31a)	155.5(2)	P(1b)–Ru(1b)–P(2b)	179.0(1)	C(51a)–C(56a)–C(55a)	120.4(8)	Ru(1b)–P(1b)–C(1b)	120.3(3)
P(1b)–Ru(1b)–N(1b)	90.0(2)	P(2b)–Ru(1b)–N(1b)	90.1(2)	Ru(1b)–P(1b)–C(2b)	113.4(4)	C(1b)–P(1b)–C(2b)	98.9(5)
P(1b)–Ru(1b)–N(11b)	88.4(2)	P(2b)–Ru(1b)–N(11b)	91.4(2)	Ru(1b)–P(1b)–C(3b)	117.4(4)	C(1b)–P(1b)–C(3b)	102.9(5)
N(1b)–Ru(1b)–N(11b)	178.1(2)	P(1b)–Ru(1b)–N(21b)	90.9(2)	C(2b)–P(1b)–C(3b)	100.8(5)	Ru(1b)–P(2b)–C(4b)	113.0(4)
P(2b)–Ru(1b)–N(21b)	88.1(2)	N(1b)–Ru(1b)–N(21b)	101.1(2)	Ru(1b)–P(2b)–C(5b)	117.0(4)	C(4b)–P(2b)–C(5b)	102.3(6)
N(11b)–Ru(1b)–N(21b)	77.9(2)	P(1b)–Ru(1b)–N(31b)	92.2(2)	Ru(1b)–P(2b)–C(6b)	117.7(3)	C(4b)–P(2b)–C(6b)	103.1(5)
P(2b)–Ru(1b)–N(31b)	88.7(2)	N(1b)–Ru(1b)–N(31b)	103.8(2)	C(5b)–P(2b)–C(6b)	101.7(5)	Ru(1b)–N(1b)–O(1b)	123.2(4)
N(11b)–Ru(1b)–N(31b)	77.3(2)	N(21b)–Ru(1b)–N(31b)	154.9(2)	Ru(1b)–N(1b)–O(2b)	120.5(5)	O(1b)–N(1b)–O(2b)	116.3(6)

Table 11 (*continued*)

Ru(1a)–P(1a)–C(1a)	112.7(3)	Ru(1a)–P(1a)–C(2a)	113.4(3)	Ru(1b)–N(11b)–C(12b)	119.7(5)	Ru(1b)–N(11b)–C(16b)	120.7(5)
C(1a)–P(1a)–C(2a)	101.1(5)	Ru(1a)–P(1a)–C(3a)	123.5(4)	C(12b)–N(11b)–C(16b)	119.5(6)	N(11b)–C(12b)–C(13b)	122.8(8)
C(1a)–P(1a)–C(3a)	100.4(5)	C(2a)–P(1a)–C(3a)	102.9(5)	N(11b)–C(12b)–N(25b)	113.3(6)	C(13b)–C(12b)–N(25b)	123.9(8)
Ru(1a)–P(2a)–C(4a)	118.4(4)	Ru(1a)–P(2a)–C(5a)	116.3(7)	C(12b)–C(13b)–C(14b)	116.4(9)	C(13b)–C(14b)–C(15b)	122.7(9)
C(4a)–P(2a)–C(5a)	96.4(8)	Ru(1a)–P(2a)–C(6a)	117.5(6)	C(14b)–C(15b)–C(16b)	116.6(9)	N(11b)–C(16b)–C(15b)	121.9(8)
C(4a)–P(2a)–C(6a)	103.0(6)	C(5a)–P(2a)–C(6a)	101.8(10)	N(11b)–C(16b)–N(35b)	112.1(6)	C(15b)–C(16b)–N(35b)	126.0(8)
Ru(1a)–N(1a)–O(1a)	125.4(5)	Ru(1a)–N(1a)–O(2a)	120.6(7)	Ru(1b)–N(21b)–C(22b)	144.3(5)	Ru(1b)–N(21b)–N(25b)	110.5(4)
O(1a)–N(1a)–O(2a)	113.7(7)	Ru(1a)–N(11a)–C(12a)	119.5(5)	C(22b)–N(21b)–N(25b)	104.6(6)	N(21b)–C(22b)–C(23b)	109.8(7)
Ru(1a)–N(11a)–C(16a)	121.3(5)	C(12a)–N(11a)–C(16a)	119.1(6)	N(21b)–C(22b)–C(41b)	125.4(7)	C(23b)–C(22b)–C(41b)	124.8(7)
N(11a)–C(12a)–C(13a)	122.4(7)	N(11a)–C(12a)–N(25a)	112.3(6)	C(22b)–C(23b)–C(24b)	106.9(8)	C(23b)–C(24b)–N(25b)	108.4(8)
C(13a)–C(12a)–N(25a)	125.2(7)	C(12a)–C(13a)–C(14a)	118.1(8)	C(12b)–N(25b)–N(21b)	118.5(6)	C(12b)–N(25b)–C(24b)	130.5(7)
C(13a)–C(14a)–C(15a)	121.3(8)	C(14a)–C(15a)–C(16a)	115.7(7)	N(21b)–N(25b)–C(24b)	110.2(6)	Ru(1b)–N(31b)–C(32b)	144.0(5)
N(11a)–C(16a)–C(15a)	123.4(7)	N(11a)–C(16a)–N(35a)	111.4(6)	Ru(1b)–N(31b)–N(35b)	109.5(4)	C(32b)–N(31b)–N(35b)	105.5(6)
C(15a)–C(16a)–N(35a)	125.2(6)	Ru(1a)–N(21a)–C(22a)	145.2(5)	N(31b)–C(32b)–C(33b)	110.2(7)	N(31b)–C(32b)–C(51b)	124.1(7)
Ru(1a)–N(21a)–N(25a)	110.2(4)	C(22a)–C(21a)–N(25a)	104.1(5)	C(33b)–C(32b)–C(51b)	125.6(7)	C(32b)–C(33b)–C(34b)	106.7(7)
N(21a)–C(22a)–C(23a)	110.5(7)	N(21a)–C(22a)–C(41a)	124.1(7)	C(33b)–C(34b)–N(35b)	106.5(7)	C(16b)–N(35b)–N(31b)	120.3(6)
C(23a)–C(22a)–C(41a)	125.3(7)	C(22a)–C(23a)–C(24a)	108.3(7)	C(16b)–C(35b)–C(34b)	128.4(7)	N(31b)–N(35b)–C(34b)	110.9(6)
C(23a)–C(24a)–N(25a)	106.8(7)	C(12a)–N(25a)–N(21a)	119.6(6)	C(22b)–C(41b)–C(42b)	123.7(7)	C(22b)–C(41b)–C(46b)	117.9(8)
C(12a)–N(25a)–C(24a)	129.5(7)	N(21a)–N(25a)–C(24a)	110.1(6)	C(42b)–C(41b)–C(46b)	118.4(8)	C(41b)–C(42b)–C(43b)	120.7(8)
Ru(1a)–N(31a)–C(32a)	144.6(5)	Ru(1a)–N(31a)–N(35a)	109.9(4)	C(42b)–C(43b)–C(44b)	120.7(9)	C(43b)–C(44b)–C(45b)	119.9(9)
C(32a)–N(31a)–N(35a)	105.3(5)	N(31a)–C(32a)–C(33a)	110.2(6)	C(43b)–C(44b)–Cl(4b)	120.6(9)	C(45b)–C(44b)–Cl(4b)	119.4(7)
N(31a)–C(32a)–C(51a)	125.3(6)	C(33a)–C(32a)–C(51a)	124.5(6)	C(44b)–C(45b)–C(46b)	120.4(9)	C(41b)–C(46b)–C(45b)	119.9(10)
C(32a)–C(33a)–C(34a)	106.1(7)	C(33a)–C(34a)–N(35a)	107.5(7)	C(32b)–C(51b)–C(52b)	121.5(7)	C(32b)–C(51b)–C(56b)	120.0(7)
C(16a)–N(35a)–N(31a)	120.0(5)	C(16a)–N(35a)–C(34a)	129.0(6)	C(52b)–C(51b)–C(56b)	118.4(7)	C(51b)–C(52b)–C(53b)	119.8(7)
N(31a)–N(35a)–C(34a)	110.7(6)	C(22a)–C(41a)–C(42a)	123.4(7)	C(52b)–C(53b)–C(54b)	119.4(9)	C(53b)–C(54b)–C(55b)	122.0(9)
C(22a)–C(41a)–C(46a)	119.1(8)	C(42a)–C(41a)–C(46a)	117.2(8)	C(53b)–C(54b)–Cl(5b)	118.2(8)	C(55b)–C(54b)–Cl(5b)	119.8(7)
C(41a)–C(42a)–C(43a)	122.3(8)	C(42a)–C(43a)–C(44a)	118.7(11)	C(54b)–C(55b)–C(56b)	119.1(8)	C(51b)–C(56b)–C(55b)	121.2(8)

(K. J. T.) for partial support of this research. We also thank Johnson Matthey Aesar/Alfa for a generous loan of $RuCl_3 \cdot 3H_2O$, Ms. Lisa F. Szczepura for her assistance with the electrochemical measurements, and Professor Kenneth A. Goldsby for many helpful discussions. Upgrade of the diffractometer was made possible by Grant 89-13733 from the Chemical Instrumentation Program of the National Science Foundation.

References

1 F. P. Dwyer and D. P. Mellor, *Chelating Agents and Metal Chelates*, Academic Press, Orlando, 1964.
2 Y. I. Kim, S. Salim, M. J. Hug and T. E. Mallouk, *J. Am. Chem. Soc.*, 1991, **113**, 9561; S. L. Mecklenburg, B. M. Peek, B. W. Erickson and T. J. Meyer, *J. Am. Chem. Soc.*, 1991, **113**, 8540; D. P. Rillema, A. K. Edwards, S. C. Perine and A. L. Crumbliss, *Inorg. Chem.*, 1991, **30**, 4421.
3 E. C. Constable, *Adv. Inorg. Chem. Radiochem.*, 1989, **34**, 1.
4 E. C. Constable and M. D. Ward, *J. Chem. Soc., Dalton Trans.*, 1990, 1405; P. J. Steel and E. C. Constable, *J. Chem. Soc., Dalton Trans.*, 1990, 1389; E. C. Constable, *Adv. Inorg. Chem. Radiochem.*, 1986, **30**, 69.
5 C. R. Heckler, P. E. Fanwick and D. R. Millin, *Inorg. Chem.*, 1991, **30**, 659.
6 R. Hage, R. Prins, J. G. Haasnoot, J. Reedijk and J. G. Vos, *J. Chem. Soc., Dalton Trans.*, 1987, 1389.
7 J.-P. Collin, S. Guillerez, J.-P. Sauvage, F. Barigelletti, L. DeCola, L. Flamigni and V. Balzani, *Inorg. Chem.*, 1991, **30**, 4230.
8 R. D. Gillard, *Coord. Chem. Rev.*, 1983, **50**, 303.
9 K. P. Seddon, *Coord. Chem. Rev.*, 1982, **41**, 79.
10 K. Kalyanasundaram, *Coord. Chem. Rev.*, 1982, **46**, 159.
11 N. Baidya, M. Olmstead and P. K. Mascharak, *Inorg. Chem.*, 1991, **30**, 929.
12 J. P. Sauvage and M. Ward, *Inorg. Chem.*, 1991, **30**, 3869.
13 G. A. Mabbot, *J. Chem. Educ.*, 1983, **60**, 697; P. T. Kissinger and W. R. Heineman, *J. Chem. Educ.*, 1983, **60**, 702.
14 C. A. Tolman, *Chem. Rev.*, 1977, **77**, 313.
15 M. A. Hitchman and G. L. Rowbottom, *Coord. Chem. Rev.*, 1982, **42**, 55 and refs. therein.
16 D. J. Jameson and K. A. Goldsby, *J. Org. Chem.*, 1990, **55**, 4992.
17 P. T. Kissinger and W. R. Heineman, *Laboratory Techniques in Electroanalytical Chemistry*, Marcel Dekker, New York, 1984.
18 (*a*) M. R. Churchill, R. A. Lashewycz and F. J. Rotella, *Inorg. Chem.*, 1977, **16**, 265; (*b*) G. M. Sheldrick, SHELXTL PLUS, Siemens Analytical Instruments, Madison, WI, 1983; (*c*) M. R. Churchill, *Inorg. Chem.*, 1973, **12**, 1213.
19 C. K. Johnson, ORTEP II, Report ORNL-5138, Oak Ridge National Laboratory, Oak Ridge, TN, 1974.
20 C. A. Bessel, R. F. See, D. L. Jameson, M. R. Churchill and K. J. Takeuchi, *J. Chem. Soc., Dalton Trans.*, 1991, 2801.
21 W. C. Wosley, *J. Chem. Educ.*, 1973, **50**, A335; K. Raymond, *Chem. Eng. News*, 1983, **61**, 4.
22 R. A. Leising and K. J. Takeuchi, *J. Am. Chem. Soc.*, 1988, **110**, 4079.
23 R. A. Leising, S. A. Kubow, M. R. Churchill, L. A. Buttrey, J. W. Ziller and K. J. Takeuchi, *Inorg. Chem.*, 1990, **29**, 1306.
24 R. A. Leising and K. J. Takeuchi, submitted for publication.
25 B. P. Sullivan, J. M. Calvert and T. J. Meyer, *Inorg. Chem.*, 1980, **19**, 1404.
26 D. W. Krassowski, J. H. Nelson, K. R. Brower, D. Hauenstein and R. A. Jacobson, *Inorg. Chem.*, 1988, **27**, 4294.
27 R. O. Roste, D. J. Cole-Hamilton and G. Wilkinson, *J. Chem. Soc., Dalton Trans.*, 1984, 2067.
28 E. J. Probitts, D. R. Saunders, D. H. Stone and R. J. Mawby, *J. Chem. Soc., Dalton Trans.*, 1986, 1167 and refs. therein.
29 M. J. Cleare and W. P. Griffith, *J. Chem. Soc. A*, 1967, 1144.
30 S. Pinchase and I. Lauchlit, *Infrared Spectra of Labelled Compounds*, Academic Press, London, 1971.
31 S. A. Adeymi, F. J. Miller and T. J. Meyer, *Inorg. Chem.*, 1972, **11**, 994.
32 H. Nagao, M. Mukaida, K. Shimizu, F. S. Howell and H. Kakihana, *Inorg. Chem.*, 1986, **25**, 4312.
33 N. Nakamoto, *Infrared and Raman Spectra of Inorganic and Coordination Compounds*, 4th edn., Wiley, New York, 1986.
34 B. A. Haymore and J. A. Ibers, *Inorg. Chem.*, 1975, **14**, 3060.
35 R. A. Leising, J. J. Grzybowski and K. J. Takeuchi, *Inorg. Chem.*, 1988, **27**, 1020.
36 R. P. Thummel and Y. Jahng, *Inorg. Chem.*, 1986, **25**, 2527.
37 J. M. Calvert, D. L. Peebles and R. J. Nowak, *Inorg. Chem.*, 1985, **24**, 3111.
38 J. M. Calvert and T. J. Meyer, *Inorg. Chem.*, 1985, **20**, 27.
39 M. J. Root and E. Deutsch, *Inorg. Chem.*, 1985, **24**, 1464.
40 M. J. Suen, S. W. Wilson, M. Pomerantz and J. L. Walsh, *Inorg. Chem.*, 1989, **28**, 786.
41 F. R. Keene, D. J. Salmon, J. L. Walsh, H. A. Abruna and T. J. Meyer, *Inorg. Chem.*, 1980, **19**, 1896 and refs. therein; H. D. Abruna, J. L. Walsh, T. J. Meyer and W. R. Murray *Inorg. Chem.*, 1981, **20**, 1481.
42 S. A. Kubow, L. F. Szczepura, C. A. Bessel and K. J. Takeuchi, unpublished work.

43 C. K. Ingold, *Q. Rev. Chem. Soc.*, 1957, **11**, 1; H. C. Brown, H. Batholomay, jun., and M. D. Traylor, *J. Am. Chem. Soc.*, 1944, **66**, 435; R. W. Taft, jun., *Steric Effects in Organic Chemistry*, Wiley, New York, 1956; T. L. Brown, *Inorg. Chem.*, 1992, **31**, 1286.
44 R. A. Harte, *Molecules in Three Dimensions*, American Society of Biological Chemists, Bethesda, MD, 1969.
45 S. H. Simonsen and M. H. Mueller, *J. Inorg. Nucl. Chem.*, 1965, **27**, 309.
46 G. R. Clark, J. M. Waters and K. R. Whittle, *J. Chem. Soc., Dalton Trans.*, 1975, 2556.
47 M. F. McGuiggan and L. H. Pignolet, *Cryst. Struct. Commun.*, 1978, **7**, 583.
48 R. A. Sanchez-Delgado, U. Thewalt, N. Valencia, A. Andrillo, R.-L. Marquez-Silva, J. Puga, H. Schollhorn, H.-P. Klein and B. Fontal, *Inorg. Chem.*, 1986, **25**, 1097.
49 S. D. Robinson and M. F. Uttley, *J. Chem. Soc., Dalton Trans.*, 1973, 1912.
50 A. C. Skapski and F. A. Stephens, *J. Chem. Soc., Dalton Trans.*, 1974, 390.
51 R. Mason, K. M. Thomas, D. F. Gill and B. L. Shaw, *J. Organomet. Chem.*, 1972, **40**, C67.
52 E. A. Seddon and K. R. Seddon, *The Chemistry of Ruthenium*, Elsevier, New York, 1984 and refs. therein.
53 C. T. Huang, J. A. Weil and B. E. Robertson, *Acta Crystallogr., Sect. B*, 1975, **31**, 914.
54 U. Thewalt and R. E. Marsh, *Inorg. Chem.*, 1970, **9**, 1604.

Received 13*th November* 1992; Paper 2/06051E